University of Neuchâtel
Institute of Physics

Mass Spectrometry with Cryogenic Detectors

Thesis by
Dominique Gritti

in partial Fullfillment of the Requirements for the Degree of
Docteur ès Sciences

Neuchâtel, October 2001

Mass Spectrometry with Cryogenic Detectors

IMPRIMATUR POUR LA THESE

Mass spectrometry with cryogenic detectors

de M. Dominique Gritti

UNIVERSITE DE NEUCHATEL

FACULTE DES SCIENCES

La Faculté des sciences de l'Université de Neuchâtel sur le rapport des membres du jury,

MM. J.-L. Vuilleumier (directeur de thèse), D. Twerenbold et H. Balsiger (Berne)

autorise l'impression de la présente thèse.

Neuchâtel, le 18 octobre 2001

Le doyen:

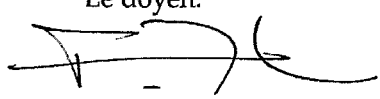

F. Zwahlen

Contents

Abbreviations

Some useful abbreviations

MS	:	Mass Spectrometry
TOF	:	Time-of-Flight
MALDI	:	Matrix Assisted Laser Desorption and Ionization
PI	:	Photon-Ionization
FAB	:	Fast Atom Bombardment
SIMS	:	Secondary Ion Mass Spectrometry
LDI	:	Laser Desorption and Ionization
ESI	:	Electrospray Ionization
SEM	:	Secondary Electron Multiplier
MCP	:	Microchannel Plate
STJ	:	Superconducting Tunnel Junction
SIS	:	Superconductor-Insulator-Superconductor
NIS	:	Normal-Insulator-Superconductor

Introduction

We will start with a historical introduction showing the main developments about ionization and desorption methods for biomolecules analyses. Then, an abstract is given about our work at Institute of physics, University of Neuchatel.

For a long time scientists have been investigating the structure of organic molecules and biopolymers. Mass spectrometry has become a powerful tool for the analysis of large molecules due to new technologies of desorption and ionization.
These different techniques are:

- Fast atom bombardment **FAB** [1]
- Secondary ion mass spectrometry **SIMS** [2]
- Irradiation with laser light pulse **LDI**

In 1988 two major breakthroughs have been made, one by Karas and Hillenkamp [3], the second by Tanaka et al. [4]. In both methods the analyte molecules were diluted in a matrix.
Tanaka et al used as matrix a liquid (glycerol) containing a fine powder of metal whereas Karas and Hillenkamp used a solid matrix consisting of low mass molecules strongly absorbing UV light. The sample is exposed to a laser pulse and the interaction between the UV light and the matrix allows the ejection of analyte molecules. The ejected molecules are ionized and can thus be analysed in a mass spectrometer.
This technique was called matrix assisted laser desorption ionization (**MALDI**) by Karas and Hillenkamp. With the MALDI technique some molecules with a mass up to 500 kDa have been successfully desorbed and ionized. MALDI is a fast and easy method to get informations about macromolecules (eg, proteins, polymers...) . This technique has also been employed as a method for a rapid identification of whole bacteria from healthy subjects [6, 7, 8, 9]

and DNA sequencing [28, 29].
It has been used with different kinds of spectrometers such as Time-of-flight(TOF), Fourier transform ion cyclotron resonance (FTICR) and magnetic sector ion trap.

An important point for the mass spectrometry whatever the experimental setup (e.g: TOF, FTICR,..) used is probably the detector itself.
The macromolecules detection is difficult with classical ion detectors (e.g secondary electron multiplier SEM, microchannel plate MCP,...), because the detection efficiency decreases strongly when the molecule velocity decreases. In order to solve this problem, D.Twerenbold proposed in 1995 [5] the use of cryogenic particle detectors previously developed for applications such as dark matter search and X ray spectroscopy.

In this thesis, we will compare the detection efficiency of classical detectors with cryogenic detectors for their use in mass spectrometry. Analysis of proteins, oligonucleotides as well as polymers have been made with different kinds of cryogenic detectors. These latters are also a powerful tool for the detection of neutral molecules. As a matter of fact, the detection method with these cryodetectors is radically different. In this case, the total energy of the incident particle is deposited into the cryogenic detector and transformed into measurable increase of the internal energy of the detector.
These cryogenic detectors have to be kept at very low temperature, typically below 1 K. There are two mains reasons for this:

- many implementations of cryogenic particle detectors require superconducting films. This effect of metallic films becoming superconducting typically occurs at temperature around a few Kelvin.
- when a large molecule with an energy of a few keV hits a surface, the main internal energy excitations of the material are phonons (lattice vibrations). Low operating temperatures are required to reduce the background of thermal phonons.

Chapter 1

Mass Spectrometry

A mass spectrometer is an instrument that separates and detects several kinds of ions by determining their Mass-to-Charge ratio.
All common mass analysers use a electric and/or a magnetic field to apply a force to ions. The relationships between force, mass and electric and magnetic field is:

$$\vec{F} = m \cdot \ddot{\vec{x}} = q \cdot \left(\vec{E} + \dot{\vec{x}} \wedge \vec{B}\right) \tag{1.1}$$

Where:

- $\vec{F}$ is the force applied on the ion.
- m is the mass of the ion.
- $\ddot{\vec{x}}$ is the acceleration.
- q is the charge of the ion.
- $\vec{E}$ is the electric field.
- $\dot{\vec{x}} \wedge \vec{B}$ is the vector cross product of the ion velocity and the applied magnetic field.

It is apparent that the force applied on the ion is ionic charge dependent and according to the Newton's law the force applied on the ion produces an acceleration which is mass dependent. This is the reason why mass spectrometers separate ions according to their *mass-to-charge ratio* m/q rather than by mass only.

1.1 Time-of-flight mass analysers

A time-of-flight mass spectrometer measures the mass of the molecules by a selection in time. Ions of different masses move from the ion source to the detector (see Figure: 1.1). The ions are accelerated into the mass spectrometer by an electric field applied to the electrodes.
With this kind of spectrometer, only one laser shot is sufficient to obtain a spectrum with all masses ($M^+, 2M^+, ...$).
More details can be obtained in [11].

The time-of-flight is given by:

$$t_{tof} = L \cdot \sqrt{\frac{m}{q} \cdot \frac{1}{2U}} \tag{1.2}$$

Where:

- t_{tof} is the time-of-flight.
- L is the drift length.
- m/q is the mass-to-charge ratio.
- U is the acceleration voltage.

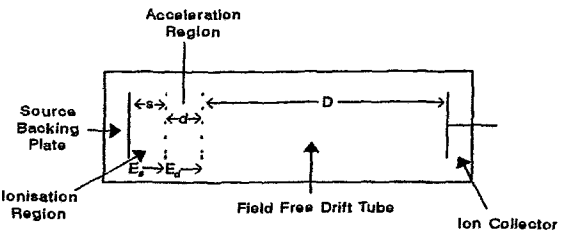

Figure 1.1: Schematic diagram of a dual stage time-of-flight mass spectrometer

Several techniques exist in order to create positif or negative ions. It may be formed in gas phase (for example, by electron impact or multiphoton ionization). Ions may also be created by laser desorption. This technique will

be studied in more details in the next chapter.

For our application, we chose to work with a MALDI-TOF mass spectrometer. This technique produces singly, doubly,... charged ions which is going to demonstrate the ability to separate the charge state of a ion with cryogenic detectors. Beside, this kind of mass spectrometer can be home-built at low cost as well as easily modifiable.

1.2 Other types of mass analysers

1.2.1 Magnetic sector mass spectrometers

Magnetic sector mass spectrometer apply a magnetic field perpendicularly to the ions direction, their velocity remains constant but the ions travel in a circular path (see Figure:1.2).

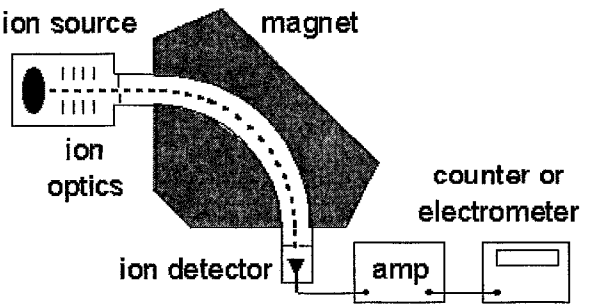

Figure 1.2: Schematic representation of the basic setup of a magnetic sector mass spectrometer.

For a magnetic sector, the relation between the mass-to-charge ratio and the ions motion is given by:

$$\frac{m}{q} = \frac{B^2 r^2}{2U} \tag{1.3}$$

where:

- m/q is the mass-to-charge ratio.

- B is the magnetic field strength.
- r is the radius of the curvature.
- U is the acceleration voltage.

In the simplest mode of operation, a magnetic sector mass spectrometer keeps the accelerating potential constant and varies the magnetic field. Several slits are placed in the ions trajectory in order to select only the desired mass-to-charge ratio. Because the ion source cannot produce a mono energetic ions beam, the mass resolution is affected.
To achieve a better resolution, a double-focusing mass spectrometer is necessary. That focuses ions according to their kinetics energy.

1.2.2 Quadrupole mass spectrometers

The quadrupole mass analyzer is a *mass filter*. Combined DC and RF potentials superimposed on a constant voltage U, are applied to the quadrupole rods. The ions enter in the mass analyser with a zig-zag path. For a given U, only a selected mass-to-charge ratio will reach the detector. All other ions will not have a stable trajectory through the quadrupole mass analyzer, they will collide into the quadrupole rods and never reach the detector. (see Figure: 1.3)

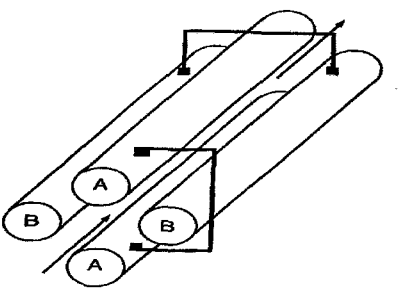

Figure 1.3: The rods A are connected and are at the same DC and superimposed RF voltages. The same is true of the rods B; however, they have an opposite DC voltage with respect to the rods A, and the RF field is phase shifted by 180°.

A derivation of the working equations for mass analyser is based upon a second-order differential equation known as the Mathieu equation [10].

1.2.3 Fourier transform mass spectrometers

In this case, the ions move onto a circular path in a magnetic field . The *cyclotron frequency* of the ion's circular motion is mass dependent. By measuring the cyclotron frequency, we can determine the mass-to-charge ratio (see Figure: 1.4) [14]. The cyclotron frequency is given by:

$$\omega = B \cdot (\frac{q}{m})^{-1} \tag{1.4}$$

Where:

- ω is the angular frequency.

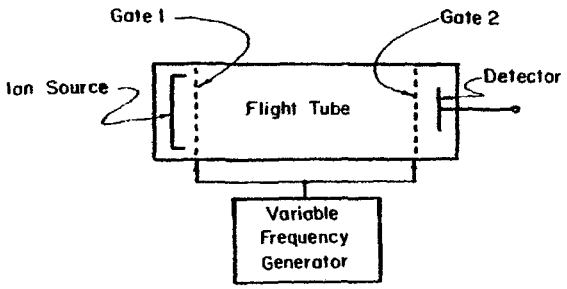

Figure 1.4: Schematic diagram of a Fourier transform time-of-flight mass spectrometer.

The ions must have the correct velocity to succesfully pass through both grids and reach the detector. A mass spectrum is recorded by modulating the frequency. The various frequencies and their relative strengths can be extracted mathematically by using a Fourier Transform which converts a time-domain signal (the image currents) to a frequency-domain spectrum (the mass spectrum).

1.3 Mass resolution in TOF mass spectrometer

In time-of-flight mass spectrometer mass resolution is improved by minimizing the initial conditions: time, space and kinetic energy distributions which degrade the resolution. In any case, a small temporal distribution can be reduce using a short laser pulse, while spatial distribution is minimized by forming ions in a small area (e.g small spot size laser). Finally, initial kinetic energy distribution is certainly the hardest parameter to eliminate. This parameter is inherent to the ionization process and nowadays still not well understood.
In the next section, we will see a method to reduce kinetic energy distribution using a reflectron.

1.3.1 Principle aspects in MALDI-TOF

As we have already seen, the main distribution in TOF mass spectrometer is leading due to the initial kinetic energy distribution.
In one dimension and with a simplified model the ions are generally created with a kinetic energy distribution δE, that means the time-of-flight given by equation 1.5 is transformed into:

$$t_{tof} = L \cdot \sqrt{\frac{m}{2} \cdot \frac{1}{qU + \delta E}} \tag{1.5}$$

Where δE is the energy distribution of the ions.

The effect of the energy distribution can be minimized by using a high electric field, the term qU being much greater than δE.
But the major breakthrough for MALDI-TOF analyser is the **reflectron**: it was invented by Mamyrin et al in 1973 [23]. The reflectron is an ion mirror which reflects the ions back. The ions with a higher energy penetrate deeper into the reflectron, thus the energy distribution is compensated because the faster ions travel a greater distance.
This compensation is ideal if the relation between the geometrical factors is verified (see figure; 1.5). In other words, the optimal focusing is achieved when the ions spend an equal time in the reflectron and in the drift region.

$$4d = L_1 + L_2 \tag{1.6}$$

Another way to improve the mass resolution is to use the delayed extraction

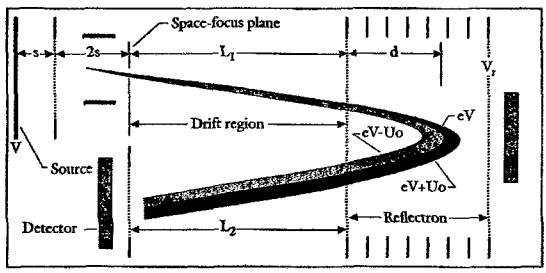

Figure 1.5: Single stage reflectron.

developed by Wiley and Mc Laren in 1955 [24].
During the time delay between ionization and extraction, ions with different initial kinetic energy will distribute themselves in the field free ion source along the extraction direction, which will convert their energy distribution into spatial distribution. This technique is also useful in order to reduce the fragmentation, especially for oligonucleotides and DNA analysis [26, 42].

1.3.2 Metastable fragmentation and its effects on mass resolution

Fragments of ion provide some structural information on the compound that is being analysed. For example, oligonucleotides fragments give an information about the arrangement of functional groups.
Fragmentation results from an excess of energy deposited in the ion during the ionization process. The rate of fragmentation depends on the excess of energy, the type of molecules and strengths of bonds. For small molecules the fragmentation occurs very prompt after ionization and for large molecules the fragmentation occurs several microsecond after the ionization, this fact is given by the large number of bonds.
The effect of fragmentation on the mass resolution and the amount of information about the molecules depends where the fragmentation occured.

- **Prompt fragmentation**

In this case, the fragmentation occurs very close (see figure 1.6 a) to the surface of desorption and the fragments have the same final kinetic energy as ions, therefore their flight times remain the same. There are not significant deterioration of mass resolution.

- **Metastable fragmentation**

The ions are fragmented during the acceleration (see figure 1.6 b), this case is the most detrimental to the mass resolution. The fragments arrive on the detector at intermediate time between the precursor and product ion masses. If an ion of mass m_1 decay at a point αS in the acceleration region to an ion of mass m_2, its time-of-flight will be given by:

$$t_{tof} = \sqrt{\frac{m^*}{2qES}} \cdot (2S + D) \tag{1.7}$$

where m^* is called apparent mass and it is given by:

$$m^* = \frac{m_1 m_2}{m_2\alpha + (1-\alpha)m_1} \tag{1.8}$$

These ions contribute to tailing of the ion peak and increase the baseline noise.

- **Post-source fragmentation**

The fragmentation occurs in the drift tube (see figure 1.6 c). Therefore, the fragments have the same velocity as their precursors and the same time-of-flight. This kind of fragmentation can give some structural information about the precursor ion. Principally, post-source fragmentation is used for oligonucleotides sequencing.

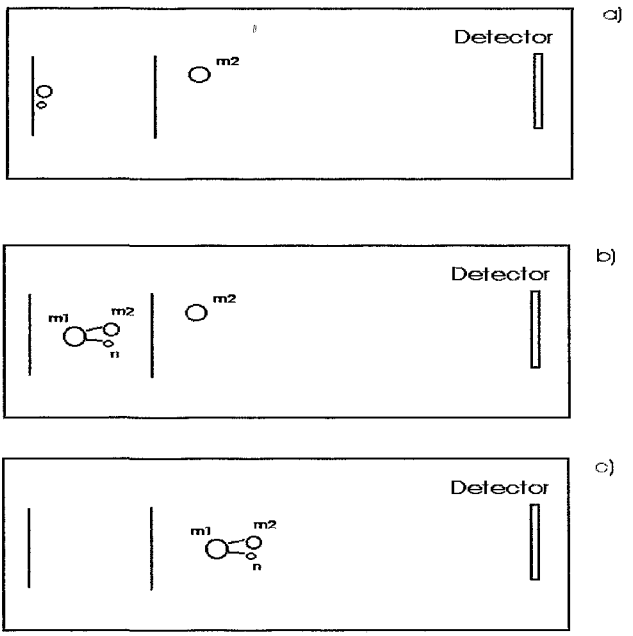

Figure 1.6: Different kinds of fragmentation which can occur in a time-of-flight mass spectrometer.

1.4 Ion Detectors

Classical detectors allow a mass spectrometer to generate a signal (current) from incident ions by creating secondary electrons or by inducing a current generated by a moving charge. Both kinds of detectors need high ion velocity (10^5 m/s) in order to create secondary electrons, whereas cryodetectors are able to detect single molecule impact with 100 % detection efficiency which is independent of the incident mass and charge state. Effectively, it is possible to detect neutral molecules with this kind of detector.

1.4.1 Electron multipliers

Detectors based on electron multiplier such as *Secondary electron Multiplier* (SEM) and *Micro Channel Plate* (MCP) are widely used because they are robust and have a large surface detection.
When an ion strikes the dynode surface, some electrons are emitted. These secondary electrons are then attracted to the next dynode where more secondary electrons are generated, ultimately resulting in a cascade of electrons (see figure: 1.7).
Their typical amplification is about 10^4 to 10^8.

1.4.2 Cryodetectors

In 1995, D. Twerenbold proposed cryogenic detectors for macromolecules detection.
The molecule detection mechanism of a cryodetector is radically different from a classical detector. A cryogenic detector measures the total energy deposited by a single molecule hitting the surface detection. A simple principle of operation of a cryodetector is illustrated on figure 1.8.

The total energy of a molecule is the product of the acceleration voltage and the charge state of molecule, which is mass independent.
These particularities are used to make a detector having 100% detection efficiency as well as a separation of charge state molecule.
The usefulness of this kind of detectors will be demonstrated in the chapter on experimental results.

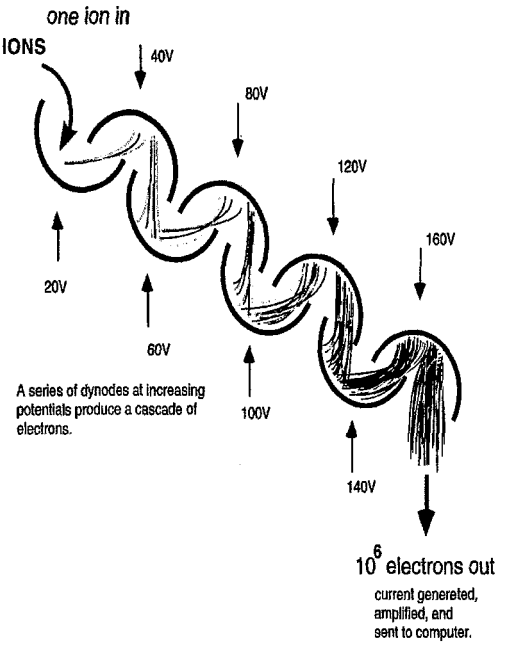

Figure 1.7: Electron multiplier and the cascade of the electrons.

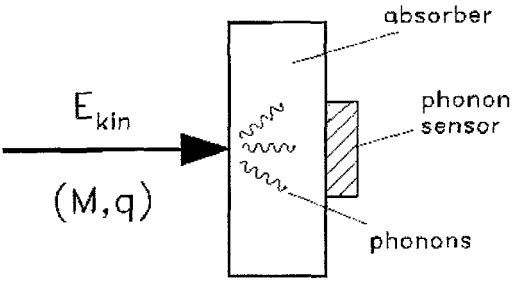

Figure 1.8: Schematic principle of a cryodetector.

Chapter 2

Desorption and Ionization Techniques

2.1 Laser desorption

The first mass spectrum measured by laser desorption has been achieved in 1970 by Vastola et al. using a pulsed laser [12].
Nowadays, this technique has been improved in order to obtain a powerful tool for MALDI method.
A laser with a certain wavelength hits the surface and the light is absorbed by the sample: the result is the creation of a plasma in which molecules are desorbed and ionized. Wavelengths used for the desorption are in the domain of UV up to mid infrared [15, 19]. By changing the wavelength, it is possible to excite differents chemical bonds. In order to desorbe whole molecules, it is necessary to adjust the laser power near the ionization threshold.

2.2 Fast Atom Bombardment FAB

With this technique, molecules are desorbed by an ion beam of Xe or Cs. Normally, the matrix used by FAB is a liquid like m-nitrobenzyl alcohol (NBA) or glycerol (see Figure; 2.1). One of the greatest disadvantage of this technique is the sensitivity. Indeed, samples require high picomole to low nanomole quantity, whereas for MALDI technique some picomoles are enough.

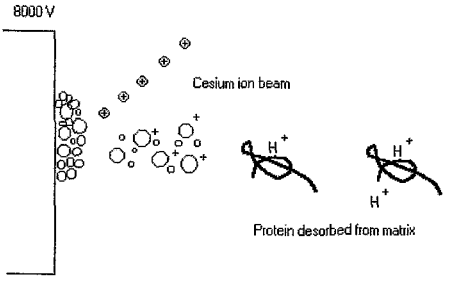

Figure 2.1: Fast atom bombardment source

2.3 Field desorption

Molecules in gas phase approach a surface of high curvature maintained at high potential in order to obtain a high potential gradient (about 10^8 V/cm). Under influence of this field, quantum tunnelling of a valence electron from the molecule to the anode leads to the creation of a radical cation.

2.4 Matrix-Assisted Laser Desorption/Ionization

In matrix-assisted laser desorption/ionization (MALDI) mass spectrometry, the proteins, peptides or synthetic polymers are dissolved in a solid or liquid matrix with low molecular weight and absorbing strongly the light of the laser. The laser pulse is typically some nanoseconds duration.
After absorbtion, matrix and analytical molecules are ejected in a gas phase, in this plume we found, neutral molecules as well as charged molecules (see Figure: 2.2).

The wavelength of the laser used for the desorption must be in the UV domain to excite the electronic state of the matrix molecules or in the medium IR to excite the vibrational states [16]. Several matrices have been tested for ultraviolet absorption: a full list can be found in [13]. As we will see later, the preparation of the samples and the launch phase is very important in order to obtain good mass spectras.

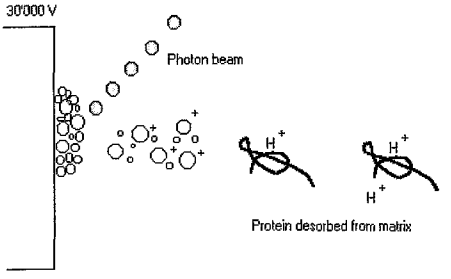

Figure 2.2: Matrix-assisted laser desorption/ionization (MALDI) source

2.4.1 Properties of Matrix

There are two major keys to achieve a good matrix for MALDI. First of all, as we have already said, the matrix must have a strong absorbance at the laser wavelength. Secondly, the solubility of the matrix, the stability in the vacuum as well as the sublimation should not occur at too high temperature. The matrix used for MALDI applications can be classified in two groups; the first one is the derivatives of the cinnamic acid such as sinapinic acid [20]. The second one are derivates of aromatic carbonyl such as 2,5 dihroxybenzoic acid (DHB) (see Figure; 2.3)

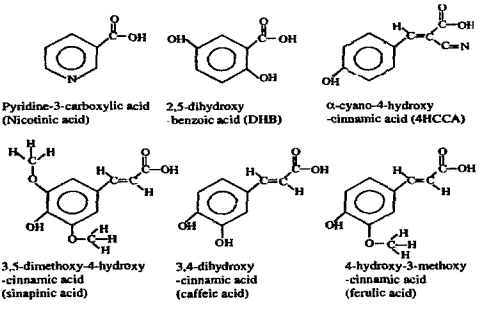

Figure 2.3: Some examples of matrices used for MALDI samples.

Both groups of matrices have a termination in carbonyl group *COOH*. Thus, UV irradiation produces a transfer of proton along H-bond. Thereby, the molecule falls in a metastable excited state.
The ratio between the matrix and the analyte is about 1000:1. Analyte is embodied in the matrix in order to lower the interaction between molecules themselves.
Some other matrices such water, glycerol and 3-NBA are used principally for liquid MALDI [17].

2.5 Mechanisms of ionization

A brief description of mechanisms of ionization [18] is presented in this chapter: these mechanisms are commonly achieved by Fast Atom Bombarbement (FAB), Electrospray Ionization (ESI) and Matrix-Assisted laser Desorption/Ionization (MALDI).

Protonation

The protonation is the addition of one or several protons in order to produce a net positive charge of +1, +2, +3,... . The most often, protonation occurs for *peptides* and *proteins* ionization. For example, $M + H^+ \longrightarrow (MH)^+$.

Cationization

The cationization is given by the addition of an ion to a neutral molecule. This ionization mechanism is especially useful with molecules which are not stable to protonation. Due to the covalent nature of proton binding, the charge can be delocalized from the proton to the molecule. This charge delocalization can destabilize the ion, resulting in fragmentation. The binding of cation as alkali, ammonium [21] with the molecule is less covalent than a proton. Therefore, the charge remains localized on the cation and usually there is less fragmentation.
A common candidate used for the cationization is *polymer* such polyethylene glycol, polystyrene,... the cation often used for the ionization is the Sodium Na^+. For example, $M + Cation^+ \longrightarrow (MCation)^+$.

Deprotonation

Deprotonation is the ejection of one or several protons in order to produce a net negative charge of -1, -2, ... This ionization is usually achieved for negative molecules such oligonucleotides. For example, $MH \longrightarrow M^- + H^+$

Chapter 3

Basics of Biochemistry and some notions about polymers characterization

3.1 Introduction: proteins and DNA

Proteins can be compared to bricks which cells and other organisms are built. In other word, we are made up by proteins.
In the same way that DNA is made up by a oligonucleotides chain (A; Adenine, C; Cytosine, G; Guanine and T; Thymine), proteins are an amino acids sequence in which the composition and the spatial configuration confers on molecules different properties.
The main goal is to understand the relation between protein structure and its function. Mass spectrometry is a powerful tool to detect the structure of a protein studying fragments created in the drift tube. Then, the obtained spectrum is compared in data base.
The sequence in which the nucleotides bases are arranged along the chain constitutes the information which determines the amino acid composition of proteins present in an organism.
The number of bases contained in a bacterium is huge, about $4 \cdot 10^6$ base pairs and for a mammal cell the number of base pairs is a $2.5 \cdot 10^9$. To study these enormous structures, the most useful methods for DNA sequencing are enzymatic restriction and *Ladder* method.
In the next sections, we are going to give only some notions about biochemistry to understand what happens in the MALDI technique and what we can learn about molecules structure.

3.2 Amino acids

As we have already seen in the chapter (2.4.1), each matrix holds a carbornyl group *COOH*. If we add an amino group NH_2 to an carboxylic acid, we obtain an ***amino acid***. For example the most common amino acid called *glycine* has the following formula;

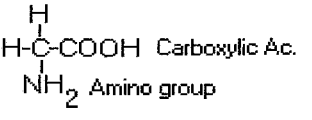

All of the 20 amino acids (See table; 3.1 p.23) are built on the same model: they have an amino group (NH_2) at one extremity and a carbonyl group at the other. Both groups are linked to the central carbon in which a hydrogen atom and a fourth group, which is called lateral group, are fixed. The only difference between all amino acids is this lateral group.
The relation between each amino acids is as follow: an amino group of one amino acid is bound to carbonyl group of the next amino acid; thereby we obtain the elimination of a molecules water and the chemical structure $-CO-NH-$ between two amino acids of a protein. We call peptide binding the binding between amino acids and therefore, the proteins are polypeptides.

3.3 Peptides and proteins

The proteins, although very different from one to an other regarding their physical and chemical properties, share a common scheme of construction. Effectively each protein is made up from amino acids. According to the number of amino acid in the sequence, we can talk of a peptide or a protein.

- Peptides have not more than 10 amino acids.
- Polypeptides are composed by 10 to 100 amino acids.
- Proteins have over 100 amino acids.

Amino Acids and Their Masses Organized According to Molecular Weight

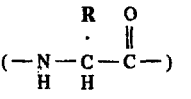

Amino acid	Letter code		Mass	R
			By mass	
Glycine	Gly	G	57	$-H$
Alanine	Ala	A	71	$-CH_3$
Serine	Ser	S	87	$-CH_2OH$
Proline	Pro	P	97	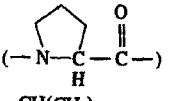
Valine	Val	V	99	$-CH(CH_3)_2$
Threonine	Thr	T	101	$-CH(OH)CH_3$
Cysteine	Cys	C	103	$-CH_2SH$
Isoleucine	Ile	I	113	$-CH(CH_3)CH_2CH_3$
Leucine	Leu	L	113	$-CH_2CH(CH_3)_2$
Asparagine	Asn	N	114	$-CH_2CONH_2$
Aspartic acid	Asp	D	115	$-CH_2COOH$
Glutamine	Gln	Q	128	$-CH_2CH_2CONH_2$
Lysine	Lys	K	128	$-CH_2(CH_2)_3NH_2$
Glutamic acid	Glu	E	129	$-CH_2CH_2COOH$
Methionine	Met	M	131	$-CH_2CH_2SCH_3$
Histidine	His	H	137	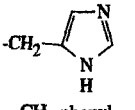
Phenylalanine	Phe	F	147	$-CH_2$-phenyl
Arginine	Arg	R	156	$-CH_2(CH_2)_2NH-C=NHNH_2$
Tyrosine	Tyr	Y	163	$-CH_2$-*para*-phenol
Tryptophan	Trp	W	186	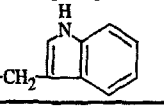

Table 3.1: List of the most important amino acids organized according to molecular weight

These values should not be taken literally. Effectively, the insulin is made up by 51 amino acids and however considered as a protein.

3.4 DNA and sequencing method

The DNA is certainly the most central substance in the working of all life on Earth.
The basic form of this molecule consists of two strands which coil around each other to make a double helix (see figure; 3.1). If we uncoil the DNA (see figure; 3.2), then each strand may be seen as a series of smaller units called *nucleotides.*

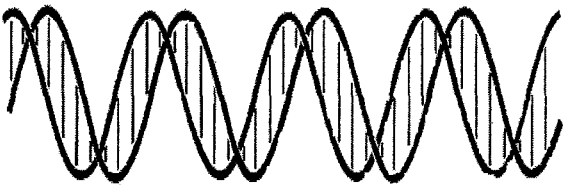

Figure 3.1: DNA double helix, showing base-pairs. The diameter of the helix is about 2 nm

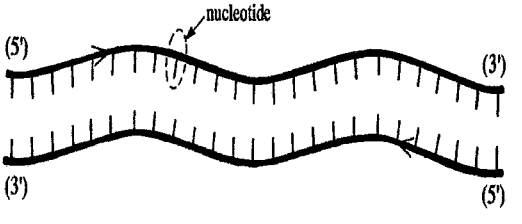

Figure 3.2: The two strands of DNA separated, showing a nucleotide.

These are linked one to another with a certain directionality named as *5'*

prime to 3' prime.
Each nucleotide is made of about 20 atoms as carbon, nitrogen and oxygen. The three parts of a nucleotide are its sugar, phosphate and base. They are labeled S, P and B in the figure 3.3.
The bases are designated by A*(Adenine)*, C*(Cytosine)*, G*(Guanine)* and T*(Thymine)*.

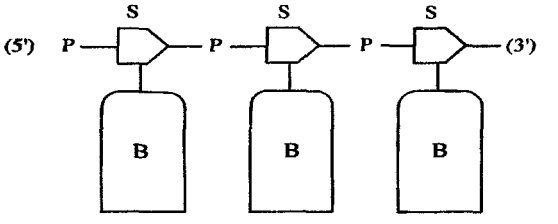

Figure 3.3: Three nucleotides showing their sugar(S), phosphate(P) and base(B) components.

A gene in the DNA tells the cell in which order to assemble these nucleotides. Because there are 20 amino acids and only 4 nucleotides, the cell has to use more than one nucleotides in the DNA to specify each amino acid in a protein (see table; 3.1).
The universal rule is that *three nucleotides* specify *one amino acid.* The table 3.2, p.28 is called *The Genetic Code*[1], it is used to determine proteins in all living things, whether they are bacteria, plants or animals.

DNA sequencing

Gel electrophoresis is the method used to analyze DNA sequence and its structure. The experimental setup is illustrated in figure 3.4 p.26.

This method can separate the DNA fragment according to their size. They carry out a net electric charge, and so they can move through a gel in the presence of an electric field.

[1]For example, a series of nucleotides such as *TTTAAAAAGGCT* specifies a portion of protein with amino acid sequence *Phe-Lys-Lys-Ala*

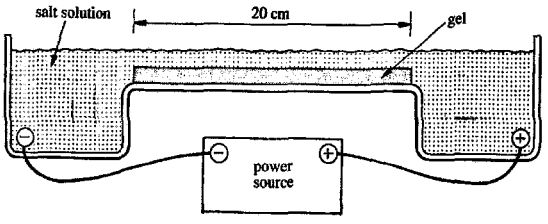

Figure 3.4: Schematic gel electrophoresis apparatus.

Usually, there are three methods used for the sequencing. The first method is to mark the gel with a dye such as ethidium bromide which becomes fluorescent under UV light when it is bound with DNA. The second method consists to implant some radioactive atoms such as phosphorus in the DNA at its 5'- or 3' ends or throughout the length of the molecule. Then the radioactive part of the DNA will become dark on an ordinary photographic film.
The last way to sequence is *restriction enzyme*, it is able to cut a specific sequence of a DNA sample. Therefore, it is possible to treat DNA with this chemical process, for example to cut only the nucleotique A. After this treatment, the DNA runs through a gel and therefore the strand is marked at every A nucleotide location. In order to locate the bases G, C and T, one can use other chemical reactions that are specific for these bases and run again these DNA fragments through the gel (see figure; 3.5 p.27).
The DNA samples analyzed by MALDI are also treated by restriction enzyme [25]. Gel electrophoresis is used for the sequencing of 400 nucleotides at maximum, beyond 400 nucleotides they cannot easily be resolved one from an other. For the sequencing of very long DNA or chromosomes[22], we have to break it into many pieces of size smaller than 400 nucleotides.

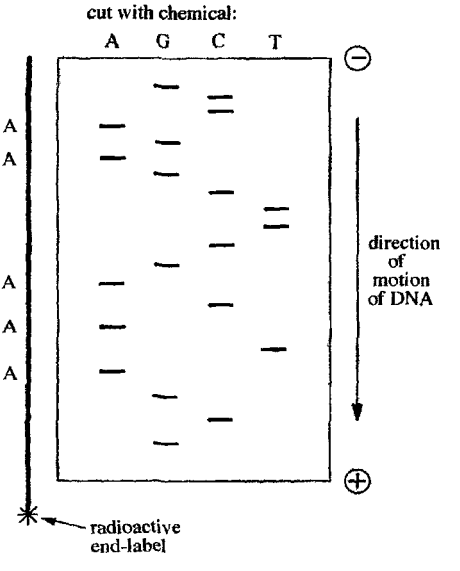

Figure 3.5: A gel for determining the sequence of a DNA molecule, which is shown in part on the left.

1st base	2nd base				3rd base
	T	C	A	G	
T	Phe	Ser	Tyr	Cys	T
	Phe	Ser	Tyr	Cys	C
	Leu	Ser	STOP	STOP	A
	Leu	Ser	STOP	Trp	G
C	Leu	Pro	His	Arg	T
	Leu	Pro	His	Arg	C
	Leu	Pro	Gln	Arg	A
	Leu	Pro	Gln	Arg	G
A	Ile	Thr	Asn	Ser	T
	Ile	Thr	Asn	Ser	C
	Ile	Thr	Lys	Arg	A
	Met	Thr	Lys	Arg	G
G	Val	Ala	Asp	Gly	T
	Val	Ala	Asp	Gly	C
	Val	Ala	Glu	Gly	A
	Val	Ala	Glu	Gly	G

Table 3.2: Any series of three bases in the DNA prescribes for an amino acid in the protein chain.The bases are always read from the left to the right. Abbreviations used: A, adenine; G,guanine; C,cytosine; T,thymine; Ala,alanine; Arg,arginine; Asn,asparagine; Asp,aspartic acid; Cys,cysteine; Gln,glutamine; Glu,glutamic acid; Gly,glycine; His,histidine; Ile,isoleucine; Leu,leucine; Lys,lysine; Met,methionine; Phe,phenylalanine; Pro,proline; Ser,serine; Thr,threonine; Trp,tryptophan; Tyr,tyrosine; Val,valine.

3.5 Characterization of polymers

MALDI-TOF technique has already demonstrated the utility for the characterization of small weight polymers [45, 46, 47].
Basically, polymers are made of a very high number of units called *oligomer*; at each extremity of the chain, there is the end group. This parameter is very important to determine the composition of the species contained in each polymer and also the different end groups present in the oligomer series [48].
To characterize polymers we have to determined the *Molecular Weight Distribution* which characterizes the distribution of each sample, namely :

- The most probable molecular weight (M_p)
- The number-average molecular weight (M_n)
- The weight-average molecular weight (M_w)
- The polydispersity index ($PD = M_w/M_n$)

Some comparison between MALDI-TOF and SEC (Size Exclusion Chromatography) are exhibited in different articles [49, 50].
Polymers can have a very high mass (until several MDa) and we know the limitation of the classical detector in this range. Several groups [50, 51] around the world have already observed this fact. Certainly cryodetectors are the solution to this problem but the sample preparation problem remains, because of the very big size of the polymers, the molecule can break up easily and only fragments are detected.

Chapter 4

Superconductivity and cryogenic detectors

In this chapter, we will see some characteritics of the superconductors in order to apply it to the cryogenic particle detectors.

4.1 The superconducting state

To be considered in a superconductor state, a material has to exhibit two distinctive properties:

- Zero resistivity $\Longleftrightarrow$ infinite conductivity is observed in a superconductor when cooled down below the critical temperature T_c (see figure; 4.1 p.32)
- The magnetic inductance drops to zero inside the superconductor when it is cooled below T_c in a weak external magnetic field. The magnetic flux is expelled from the interior of the superconductor. This effect is called *the Meissner-Ochsenfeld effect* (See figure; 4.2 p.32).

When we cool a superconductor below the critical temperature T_c, the gas of the "repulsive" individual electrons which characterizes the normal state transforms itself into a different type of fluid: it becomes a quantum fluid of highly correlated pairs of electrons (in the reciprocal momentum space **not** in the real space). These pairs are called **Cooper pairs**.
The "glue" is provided by the elastic waves of the lattice, called **phonons**.
The "distance" between the two electrons of the Cooper pair is called the coherence length ξ.

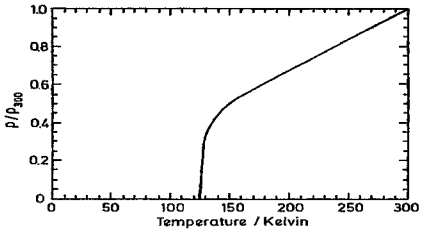

Figure 4.1: Critical temperature of an oxide superconductor $Tl_2Ba_2Ca_2Cu_3O_{10}$

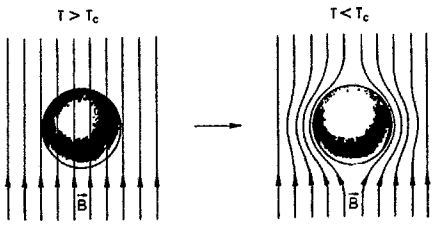

Figure 4.2: Meissner effect of a superconductor.

4.1.1 The wavefunction of the superconducting state

A Cooper pair has twice the charge of a electron, $q = 2 \cdot e$. The electrons are fermions which obey the Fermi-Dirac statistics and the Pauli exclusion principle allows only one electron in a given state. As we discussed before, Cooper pairs are composed of two electrons with opposite wave vectors $\vec{k} \uparrow, -\vec{k} \downarrow$ [1], therefore considered as bosons. Thus Cooper pairs obey the Bose-Einstein statistics and are allowed to be in the same state. Therefore the Cooper pairs are described by a unique wavefunction given by:

$$\psi(\vec{r}) = \sqrt{n_s(\vec{r})} \cdot e^{i\varphi(\vec{r})} \tag{4.1}$$

Where $n_s(\vec{r})$ is the density of Cooper pairs and $\varphi(\vec{r})$ is a spatially varying phase. [2]

[1] The symbol $\uparrow$ denotes spin up and corresponding $\downarrow$ spin down

[2] It is important to note that $\psi(\vec{r}) \cdot \psi(\vec{r})^* = n_s(\vec{r})$

4.2 BCS theory

The BCS theory has been developed by J. Bardeen, L. Cooper and J. Schrieffer in 1957 [30]; it describes well superconductivity. We will give some of the main results about this theory in order to understand the cryogenic detectors behaviour.

As we have already said, the attractive force between the two electrons making a Cooper pair is provided by the lattice vibration *phonons*. The highest possible phonon energy is given by the Debye energy $\hbar\omega_D$, it is about 10 meV. It means that only a fraction of the conduction electrons can be paired with a phonon exchange, actually only those in a shell of thickness $\pm\hbar\omega_D$ around the Fermi energy.

The BCS ground state is characterized by a wavefunction $\psi(\vec{r})$ (eq; 4.1) and a ground state energy (Cooper pairs level) which is separated from the quasiparticles state (single electrons) by an energy gap Δ (See figure; 4.3). In

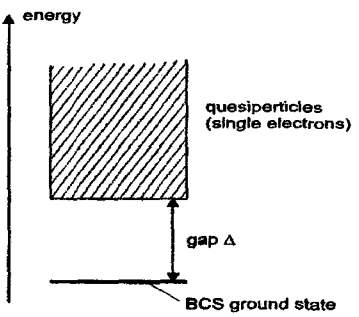

Figure 4.3: Ground state separated from the quasiparticles state by an energy gap Δ

order to break a Cooper pair, an energy of 2Δ is necessary. The energy gap of a superconductor, contrary to the semiconductor, depends on temperature (see figure; 4.4). One of the most important equation of the BCS theory is the relation between the energy gap at $T = 0$, the Debye frequency ω_D and the electron-phonon interaction potential V_0

$$\Delta(0) = 2\hbar\omega_D \cdot e^{-\frac{1}{V_0 N(E_F)}} \tag{4.2}$$

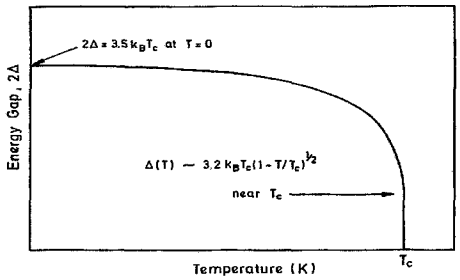

Figure 4.4: Temperature dependence of the energy gap $\Delta(T)$

$N(E_F)$ is the density of electron states at the Fermi level and V_0 is the strength of its attractive potential.
The critical temperature is given by a similar expression:

$$k_B T_c = 1.14\hbar\omega_D \cdot e^{-\frac{1}{V_0 N(E_F)}} \tag{4.3}$$

Combining these two equations, we arrive at an important relation between the energy gap at $T = 0$ and the critical temperature:

$$\frac{2\Delta(0)}{k_B T_c} = 3.52 \tag{4.4}$$

Close to T_c the energy gap $\Delta(T)$ can be approximated by

$$\frac{\Delta(T)}{\Delta(0)} = 1.74\sqrt{\left(1 - \frac{T}{T_c}\right)} \qquad for \qquad T \leq T_c \tag{4.5}$$

4.3 Thermal properties of superconductors

In the next chapter, we will see the thermal properties of different materials. Of course the superconductors properties are the most important for our applications.

4.3.1 Heat capacity

The heat capacity per mole of a normal metal at low temperature is given by:

$$C(T) = \gamma \cdot T + A \cdot T^3 \tag{4.6}$$

The coefficients γ and A can be calculated with the free electron gas model. The first term proportional in T is due to the conduction electrons, the cubic term from the lattice vibration (phonons). We find that at room temperature the heat capacity of a metal is dominated by the phonon heat capacity and usually at low temperature ($\leq 10K$) the electronic heat capacity becomes more important than the phonon heat capacity.

For the superconducting metals, the heat capacity changes radically when the temperature is below the critical temperature T_c.
First, the term due to the phonons is still unchanged, because it is not influenced by the transition to the superconducting state. It is still a cubic term with the same coefficient $C_{ph,s} = C_{ph,n} = A \cdot T^3$.
In the superconducting state the electrons condense in the same state and of course the entropy is smaller than in normal state. Therefore, the electronic heat capacity in the superconducting state vanishes very rapidly above T_c. In other words, the total heat capacity in the superconducting state is given by:

$$C_{tot,s}(T) = B \cdot e^{-\frac{\Delta}{k_B T}} + A \cdot T^3 \tag{4.7}$$

In figure 4.5 , we can see the electronic heat capacity of the superconductor changing at T_c.

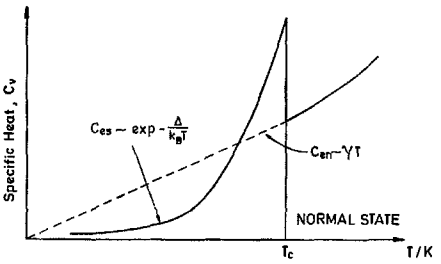

Figure 4.5: Electronic heat capacity of a metal in the normal and superconducting state.

For a dielectric crystal, the heat capacity at low temperature has a dependence in T^3

$$C_{dielec}(T) = A \cdot T^3 \tag{4.8}$$

For this reason, it is more convenient to take a dielectric as a absorber than a normal metal.

4.4 Cryogenic particle detectors

Cryogenic particle detectors [61] have been studied since many years, in order to give a very sensitive detector for some physic applications, such as X-ray spectroscopy, cold dark matter search [31] or 2β desintegration [32].
A superconducting detector has an energy gap of the order of meV, much less than semi-conductor detector (e.g Si, Ge have a gap of the order of eV). For a given energy deposition, one thus expects about 1000 times more charge than the classical detector. If E is the energy of the incident particle and Δ the energy gap of the superconductor, the quasiparticles excess created is given by:

$$N_{qp} \simeq \frac{E}{\Delta} \tag{4.9}$$

4.4.1 Basic principles

The energy E deposited by a particle in the detector will produce a temperature rise ΔT given by:

$$\Delta T = \frac{E}{C(T)} \cdot e^{-(t/\tau)} \qquad with \qquad \tau = \frac{C(T)}{G(T)} \tag{4.10}$$

where C(T) is the heat capacity of the absorber and G(T) is the thermal conductance of the link between the absorber and the heat sink (see figure; 4.6). The temperature rise ΔT induces a change of the state in the tem-

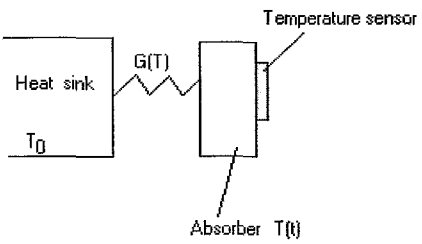

Figure 4.6: Basic components of bolometers.

perature sensor. Often the temperature rise produces a transition between the normal and the superconducting state, for example for Transition Edge Sensor (TES). The Superconducting Tunnel Junctions (STJ) are based on an other principle and will be studied in more details in the chapter 4.4.3.

4.4.2 Transition edge sensors

The temperature sensor transition edge sensor (TES) has been developed in 1990 by the Stanford group[33]. TES are fabricated by evaporation of a thin superconductor film on the absorber (see figure; 4.7).

The transition between the normal and the superconducting state gives

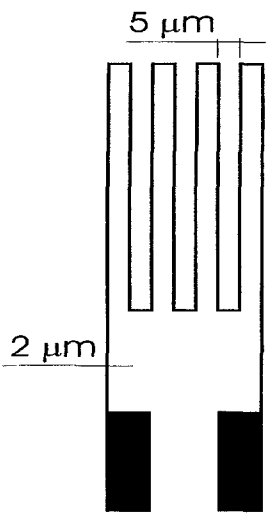

Figure 4.7: Meander patterns of a transition edge sensors.

a very sensitive thermometer. TES response is translated by the circuit in figure 4.8. When R(T) increases owing to the temperature rise, more current is forced to the coil L and thus induces a magnetic flux change which is measured with the SQUID.

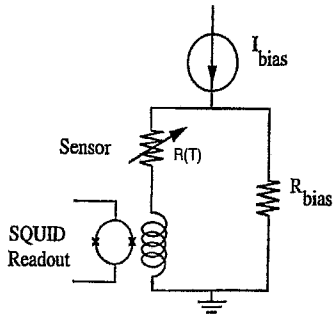

Figure 4.8: Schematic read out of a transition edge detector.

The working point is stabilized just below the transition by an electrothermal feedback (ETF) [34] (see figure; 4.9).

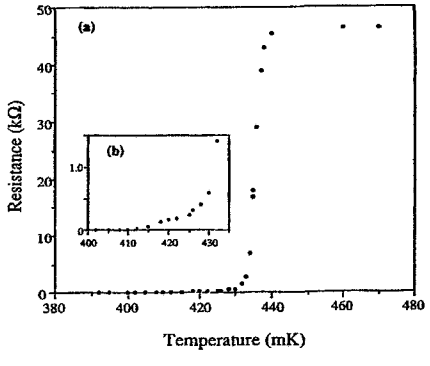

Figure 4.9: Resistive transition for a titanium transition edge sensor. (source [33])

4.4.3 Superconducting tunnel junctions

Superconducting Tunnel Junction (STJ) is an other temperature sensor developed in 1960 by I. Giaver [35, 36]
STJ consist of two thin films of superconducting material, separated by an insulator. At temperatures above the T_c, two kinds of current will settle.

- DC Josephson current given by the Cooper pairs, even if the voltage matches zero. A magnetic field is applied in order to suppress it.
- Quasiparticles current due to the tunnelling through the thin oxide barrier.

The tunnelling time can be evaluated using Fermi's Golden Rule. The energy dependence of the density of states n_s in a superconductor near the energy gap (2Δ) is given by the BCS theory as:

$$n_s(E) = n_n(E_F) \cdot \frac{\mid E - E_F \mid}{\sqrt{(E - E_F)^2 - \Delta^2}} \tag{4.11}$$

where n_n is the density of states in the normal conducting phase and E_F the Fermi energy .
The tunnelling time τ_{tun} is given by:

$$\tau_{tun} = R_N e^2 N_n(E_F) S d \tag{4.12}$$

where R_N is the normal resistance, e the electron charge, $N_n(E_F)$ the density of states in the normal conducting phase at Fermi energy, S the junction overlap and d the thickness of the barrier.

For a voltage bias V between $\frac{k_B T}{e} << V < \frac{2\Delta}{e}$ the thermal current I_{th} is proportional to $N_{th} \cdot \tau_{tun}$. Here, the density of quasiparticles N_{th} is proportional to $\sqrt{T} \cdot exp - (\Delta / k_B T)$ given by the Boltzmann statistics. The current of quasiparticles is reduced by the fact that quasiparticles can recombined in Cooper pairs with phonon emission. Therefore, the thermal recombination time is given by:

$$\tau_R = \alpha \sqrt{T} \cdot e^{-\frac{\Delta}{k_B T}} \tag{4.13}$$

This parameter can be reduced by operating the detector at low temperature, typically $1/10 \cdot T_c$
The collected charge can be described by [37, 38].

$$Q_{eff} = \frac{E}{\Delta} \cdot \frac{\tau_{tun}^{-1}}{\tau_{tun}^{-1} + \tau_R^{-1} + \tau_x^{-1}} \tag{4.14}$$

where E is the energy deposited by the particle, τ_x is a parameter for phonon losses to the substrate and quasiparticle diffusion and $\tau_{tun}, \tau_R, \tau_x$ are explained above.

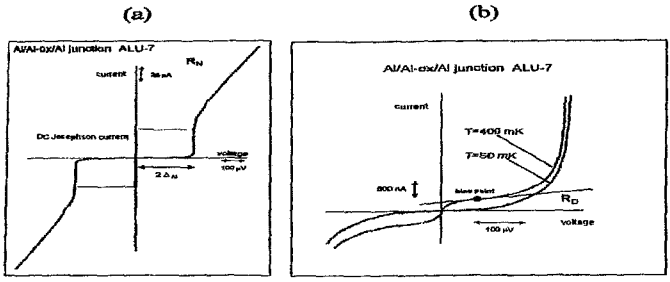

Figure 4.10: I-V curve of aluminium junction.

A typical I-V curve of SIS junction is illustrated in figure 4.10. The dynamic resistance R_D is by definition $R_D = \partial V/\partial I$. The latter must be at least a few $k\Omega$ to match the impedance of the FET. To measure an electrical signal, the STJ is usually biased $V_{bias} < \frac{2\Delta}{e}$. An interesting fact is that if a particle is absorbed in film 1 or film 2, the current has the same sign as shown in figure 4.11.

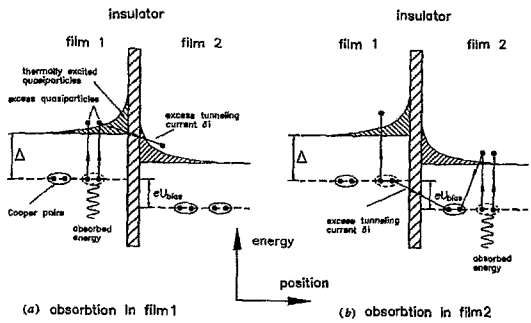

Figure 4.11: In process (a) a quasiparticle tunnels from film 1 to film 2 and in process (b) the situation is more complex, a quasiparticle tunnels from film 1 to film 2 where it recombines with a quasiparticle in film 2 to form a Cooper pair. In any case, the quasiparticles currents tunnels in the same direction.

4.4.4 Tantalum strips used as cryodetectors.

The basic idea is to use the response of a superconductive films, when a X-ray or a particle hits the film.
Due to the localized energy deposition, quasiparticles diffusion occurs and they reach tunnelling junctions placed at both extremities of the film [54, 55].
A schematic layout of one strip is illustrated on figure 4.12.

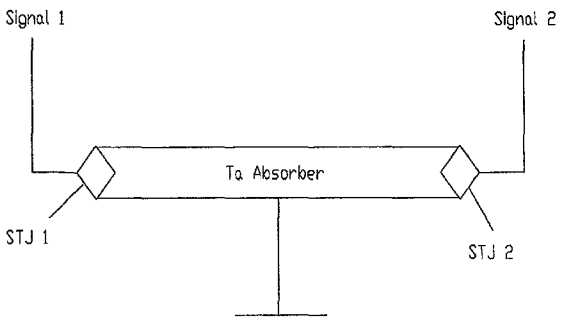

Figure 4.12: Schematic layout of one strip. At both extremities one STJ is located to collect the quasiparticles induced in the absorber by an event.

The time and diffusion of the energy carried by the quasiparticles are governed by the Chang-Scalpino equations [56] not shown in this paper.
An important parameter about the quasiparticles diffusion is the diffusion length:

$$\Lambda = \sqrt{D_{abs} \cdot \tau_{eff}} \tag{4.15}$$

where D_{abs} is the diffusion rate and τ_{eff} is the effective lifetime of the quasiparticles.
To calculate the collected charge Q_1 and $Q2$ by each junction, the superconductive film can be approximated as a 1-dimensional chain. With this model the quasiparticles diffusion is described by the differential equation [57]:

$$\partial_t n(x,t) - D\partial_x^2 n(x,t) + \frac{1}{\tau_{eff}} n(x,t) = 0 \tag{4.16}$$

where

- D is the diffusion constant
- τ_{eff} is the effective lifetime of the quasiparticles
- n(x,t) is the quasiparticle density

With adequate boundary conditions, the differential equation can be solved. The solution for the total charge Q_0 produced by the impact of a X-ray or a particle is given by:

$$Q_0^2 = Q_1^2 + Q_2^2 + 2Q_1Q_2\cosh(\alpha) \tag{4.17}$$

where

- Q_1, Q_2 are the charges collected by each junction.
- α is a the parameter $\alpha = \frac{l}{\sqrt{D \cdot \tau_{eff}}}$
- l is the length of the absorber

An X-ray spectrum is shown on the figure 4.13 and fitted with equation 4.17. Some events are due to the substrate because some phonons may reach the absorber with sufficient energy to break Cooper pairs. The events which hit directly the absorber induced two signals correlated as illustrated in figure 4.14.
This kind of detector gives in addition a information on the position of the event in the absorber. More details about this fact can be found in reference [57].

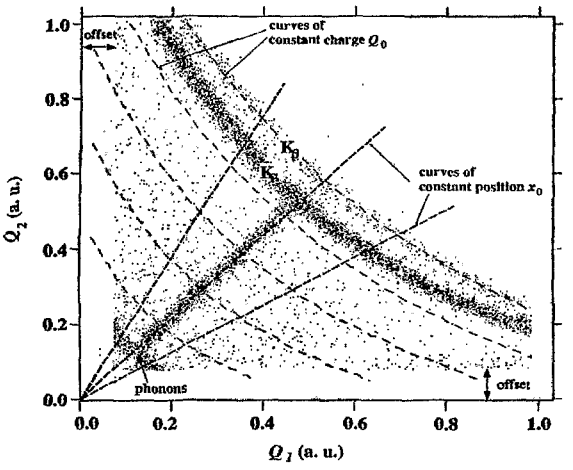

Figure 4.13: Scatter plots of Q_1 versus Q_2.The parameter α for the best fit is $\alpha = 1.6$. The K_α and K_β energy are clearly separated. (source [54])

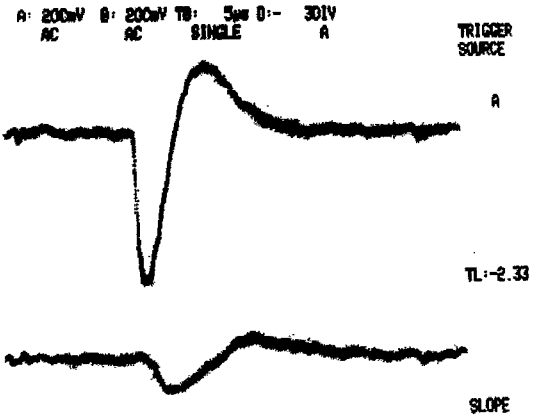

Figure 4.14: X-rays (6 keV) correlated signal induced in tantalum strip. Trigger is on channel A (signal up)

Chapter 5

Experimental set-up

5.1 Fabrication of Aluminium junctions

In the past we made superconducting tunnel junctions with tin by shadow mask technique [39]. Later, we switched to aluminium junctions to get thermally recyclable detectors. In order to do much finer geometry, we changed to photolithographic techniques.
Aluminium junctions are evaporated in our e-gun evaporation station [40]. The pressure inside the station is kept at 10^{-10} mbar by a turbo molecular pump (1000 ls^{-1}). The thickness of the first aluminium layer is 200 nm, then the substrate is transferred into the load-lock in order to do the oxide layer. The substrate is kept for 30 minutes in a oxygen atmosphere at the pressure of 3 mbar. After that, the second aluminium film is evaporated with a thickness of 150 nm.

5.2 Tantalum junctions

Besides our own detectors, we also tested devices made outside. First, we obtained tantalum junctions arrays from Oxford Instruments Scientific Research Division (Cambridge, UK).
STJ are made from $Ta/Al/AlO_x/Al/Ta$ with a tantalum epitaxial layer, the RRR of the layer being 46 [59, 60].
Detectors are placed on a target as illustrated in figure 5.1. For the experiment different dimensions of junctions have been chosen as following: $50\mu m, 100\mu m, 150\mu m, 200\mu m$.

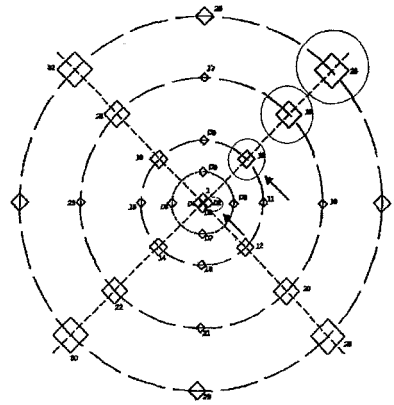

Figure 5.1: Layout of tantalum STJ. The STJ which were used are surrounded.

5.3 Tantalum strips

These detectors have been fabricated by Paul Scherrer Institut (PSI): there are 8 strips (16 junctions). A strip is illustrated on the figure 5.2 p.47.

Two junctions ($30\mu m$ x $30\mu m$) at both extremities receive a signal induced by a particle in the tantalum layer. The strip consists of an epitaxial tantalum layer 400 μm long.

To reduce the quasiparticles diffusion out of the tunnel volume into the contact pads, two aluminium layers ($Al - Al_2O_3 - Al$) are fabricated. The quasiparticles created by energy absorption in the tantalum absorber diffuse into the aluminium layer and they stay trapped because of the smaller energy Al gap relative to the tantalum [57].

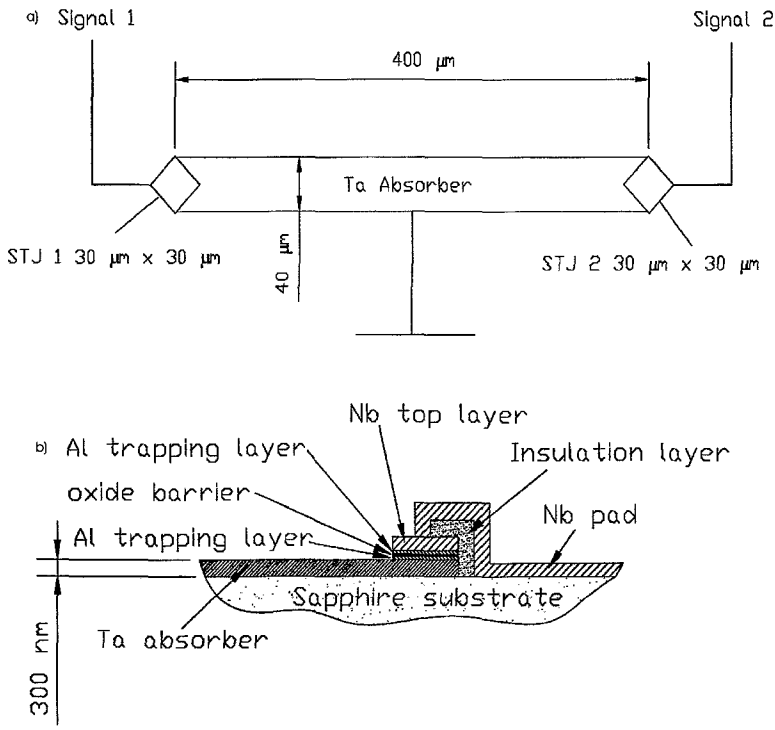

Figure 5.2: a) Junctions are made of by $Ta/Al/AlO_x/Al/Nb$ layers with a dimension of $30\mu m$ x $30\mu m$. The epitaxial tantalum absorber is $400\mu m$ long on sapphire. b) Cross section of tantalum strips (Source [54]) used in this work. The Aluminium layers create a quasiparticles trapping due to their small energy gap.

5.4 Dilution refrigerator

A Kelvinox 25 dilution refrigerator has been modified by including a side access arm which connects the dilution to the mass spectrometer. The latter is made of three concentric cylindrical cooling shields to reduce the thermal radiation (see figure; 5.3). Two small holes (5 mm diameter) through allow the macromolecules to reach the detector.

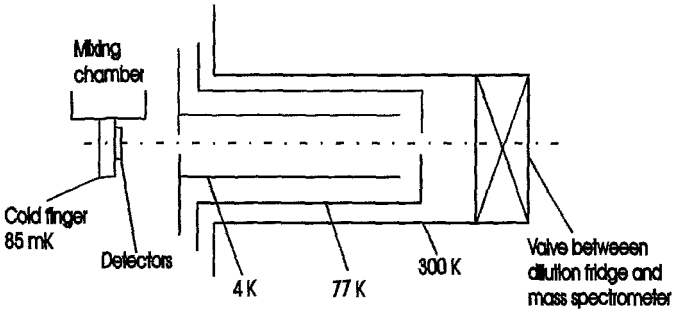

Figure 5.3: Schematic illustration of the side access arm.

With this configuration, the base temperature of the mixing chamber is 85 mK when exposed to room temperature. But the cryodetectors mounted on the cold finger have a temperature of about 600 mK due the infrared radiation.
In order to calibrate the macromolecules response, an X-rays source (^{55}Fe)[1] is mounted on the cold finger just in front of the junctions.
Superconducting coils (Nb-Ti) are mounted in the dilution to suppress the DC Josephson current.

5.5 IPH MALDI-TOF

The basic experimental set-up is illustrated in figure 5.4 p.52.

The laser generates a short laser pulse at 337 nm,[2]the attenuation can be controlled by a variable circular gradient neutral density filter. The spot size on the target is $100\mu m \times 150\mu m$. The position of the laser spot on the

[1]The main lines are $K_\alpha = 5.89keV$ and $K_\beta = 6.49keV$
[2]A nitrogen laser from Starna LSI, 337 nm, pulse duration 3 ns and $300\mu J$ per pulse.

sample can be visualized with a CCD camera.
The pressure in the mass spectrometer is kept at $5 \cdot 10^{-7}$mbar by a turbo-molecular pump. The high voltages are provided by two power supplies: [3], in positive mode the maximum voltage is + 25 kV and in negative mode -23 kV. An einzel lens is mounted in the spectrometer to focus the beam on the detector. Deflection plates are used to lead the beam and to kick off the light molecules by applying a short voltage pulse on it.
The mass spectrometer is coupled to an ionic pump in which is included a secondary electron multiplier (SEM)[4]. To work with the cryogenic detectors, the mass spectrometer is connected to the dilution fridge Oxford Kelvinox $25\mu W$ described in section 5.4.

5.5.1 Read-out

The signal is amplified by an Icarus A preamplifier of charge at room temperature as illustrated in figure 5.5 p.53. Five coaxial wires enable the connection between the read-out box and the junctions, one wire being used for the junction common point. Four channels are now operational and allow the translation of four individual junctions. A bias current can be applied individually on each junctions as well as a shock to remove the magnetic trapped flux.

5.5.2 Data acquisition

To compare the data obtained with the cryodetector and the classical detector (SEM), two programs have been developed because the data analyse is different between both detectors as we will show it in the next sections.
In any cases, the signal induced by excess quasiparticles is amplified by a charge preamplifier and digitalized by a transient recorder for analysis.

Classical detector (SEM)

For the classical detector, the data analysis is simpler than for the cryodetectors. Effectively, the raw data are sampled with Gage card acquisition [5] and therefore each spectrum obtained by a laser shot is stored on a personal computer and summed. Later on, an 8-bit analog to digital card converts the signal with a choice of 2, 5 10 MHz sampling rate.

[3]Power supplies *FUG* HCN 140-35000
[4]ETP electron multipliers, model AF820
[5]Gage Applied Sciences Inc.

Signal junction is transferred to a personal computer, 2 Gage cards are necessary to get the information from the four junctions connected in the dilution. Sampling rate can be chosen between 1, 2 , 5, 10, 20 MHz. The rise time of the signal is given by the physics of the superconducting tunnel junctions explained in the chapter 4. A typical X-ray pulse is displayed in the figure 5.6 p.53, the rise time is about $2\mu s$ and the decay time is about $20\mu s$, depending on parameters of the electronics.

Therefore, we need an analysis program to seek the peaks and select a point at fifty percent of the rise time, defined as arrival signal of the molecule.

5.5.3 Delayed extraction

Our delayed extraction box is made with two fast high voltage switches as illustrated in figure 5.7 p.53. One of the FET transistor [6] is used for the acceleration electrode and the other one for the second electrode. We can switch up to 30 kV with a rise time of 30 ns. We have measured that the turn-on delay time of our system is 210 ns. The real delay time can be selected by a pulser (100 ns to $10\mu s$) which is also used for the trigger.

5.6 Sample preparation

One of the most important aspects of the MALDI method is sample preparation. Several techniques have been tested with more or less success. More details on the sample preparation can be obtained in the references [41, 42].

Proteins [7] are dissolved in 0.1% trifluoroacetic acid (TFA) at concentration 1 mg/ml. The matrix (sinapinic acid 224 Da) is dissolved in a mixture of either ethanol ($600\mu l$) and water ($400\mu l$) at concentration 10 mg/ml.
Sometimes, the samples are dried on nitrocellulose surface to reduce the interaction between the sample holder, normally made from stainless steel, and the proteins. This preparation improves the signal intensity.

Polyethylene glycol [8] is dissolved in water at concentration 5 mM. The cationization is favoured by a solution of NaCl at 0.1 M dissolved in water, the

[6] Behlke Electronic HTS 301, Germany

[7] Insulin 5734 Da; Lysozyme 14'300 Da; Bovine Serum Albumin (BSA) 66'500 Da; Anti-Mouse Immunoglobulin IgG 135'000 Da

[8] PEG 1'500; PEG 3'000; PEG 4'000; PEG 6'000; PEG 8'000; PEG 12'000; PEG20'000; PEG 35'000 From Fluka and PEG 15000 from Merck

matrix used for PEG is 2.5 Dihydroxybenzoic acid (DHB 154 Da) at concentration 10 mg/ml dissolved in tetrahydrofuran (THF).

Polystyrene [9] is dissolved in THF at concentration 10 mg/ml. A solution of Silver Trifluoroacetate (TFAr) is used for cationization 100 mg/ml, the matrix Dithranol (1,8,9-Anthracenetriol 226 Da) is used with a concentration 10 mg/ml in THF. The matrix, the PS and the TFAr are mixed in a ratio 8:1:1.

Oligonucleotides 40-mer, 70-mer, 100-mer and 120-mer [10] are dissolved in water to make aliquots:

- 40-mer (12'373 Da): $86.5 pmol/\mu l$
- 70-mer (21'707 Da): $66 pmol/\mu l$
- 100-mer (31'075 Da): $68 pmol/\mu l$
- 120-mer (37'309 Da): $48 pmol/\mu l$

In some cases citrate ammonium 0.1 M is added for a better deprotonation. The matrix is obtained dissolving 3-Hydroxypicolinic acid (3-HPA) in 50% aqueous acetonitrile (ACN).
A detection improvement of oligonucleotides can be obtained preparing the sample on Nafion [11] layer.

[9] PS 2'000; PS 20'000; PS 20'0000; PS 200'000; PS 2'000'000

[10] **40**-mer TTT TGA TTG ATT GAT TGA TTG ATT GAT TGA TTG ATT GAT T; **70**-mer TTT TGA TTG ATT GAT TGA TTG ATT GAT TGA TTG ATT GAT TGA TTG ATT GAT TGA TTG ATTGAT TTT; **100**-mer TTT TGA TTG ATT GAT TGA TTG ATT GAT TGA TTG ATT GAT TGA TTG ATT GAT TGA TTG ATT GAT TGA TTG ATT GAT TGA TTG ATT GAT TGA TTG ATT GAT TGA TTG ATT; **120**-mer TTT TGA TTG ATT GAT TGA TTG ATT GAT TGA TTG ATT GAT TGA TTG ATT GAT TGA TTG ATT GAT TGA TTG ATT GAT TGA TTG ATT GAT TGA TTG ATT GAT TGA TTG ATT GAT TGA TT from Microsynth Schutzenstrasse 15 CH-9436 Balgach Switzerland.

[11] Nafion Perfluorinated Ion-Exchange resin, 5 in water

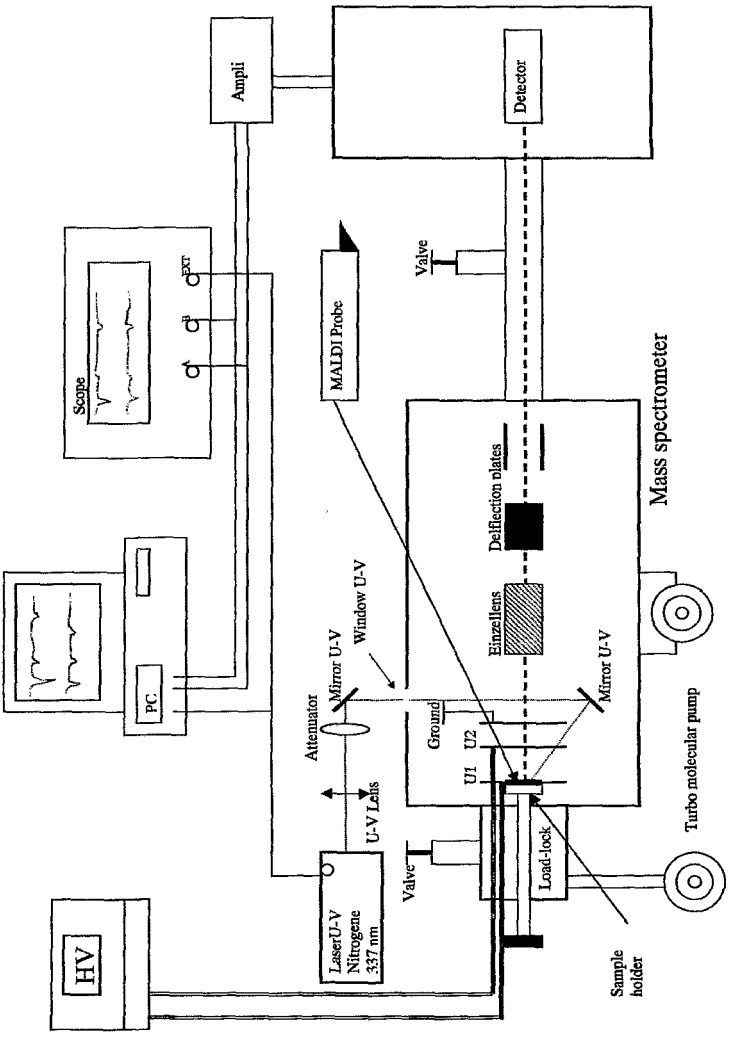

Figure 5.4: Schematic illustration of the experimental set-up.

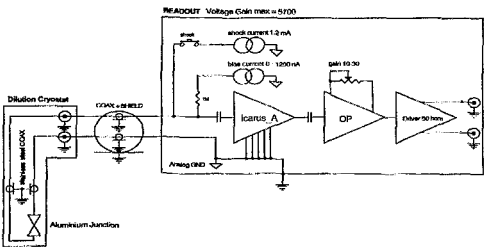

Figure 5.5: Simplified scheme of the read-out electronics.

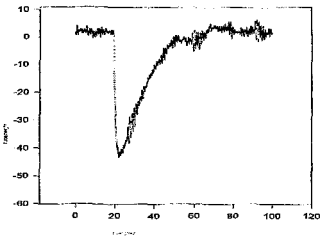

Figure 5.6: 6 keV X-ray pulse obtained after preamplification.

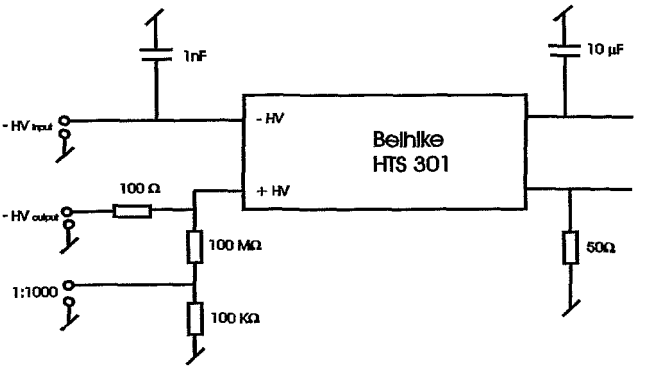

Figure 5.7: Basic components of a delay extraction.

Chapter 6

Experimental results

The first macromolecules were detected with cryodetectors in 1996/97 in Neuchatel [44]. Improved results were obtained later on by NIST/ Neuchatel/ GMU collaboration the results have been published in 1998 [43].

Most of the results presented in this chapter have been taken with an array of aluminium STJ fabricated in our laboratory as described in section 5.1. OXFORD's tantalum STJ were also tested with macromolecules. This kind of junctions is very interesting because of their very high T_c.
Tantalum strips provided by Paul Scherrer Institut (PSI) have been also tested in our dilution refrigerator with different kinds of macromolecules.

Cryodetectors are mounted in the dilution fridge and kept at 80 mK. In fact, the detector has a temperature of 600 mK due to the thermal radiation: it is used itself as a thermometer.
A X-ray source (^{55}Fe) is placed in front of the detectors to obtain an energy calibration. A X-ray spectrum is shown in figure 6.1.

The distance between the ions source and the cryodetectors is 1.6 m. The time-of-flight is given by:

$$t_{tof} = D \cdot \frac{f_0}{v_n} \tag{6.1}$$

where

$$v_n = \sqrt{2 \cdot q \cdot \frac{V}{m \cdot m_p}}$$

$$f_0 = 1 + \left(2 \cdot d_a \frac{\sqrt{y}}{D}\right) + 2 \cdot \left(\frac{d_0}{D}\right) \cdot \left(\frac{y}{y-1}\right) \cdot \left(1 - \frac{1}{\sqrt{y}}\right) \qquad and \qquad y = \frac{V}{V - V_1}$$

These values are defined as illustrated in figure 6.2.

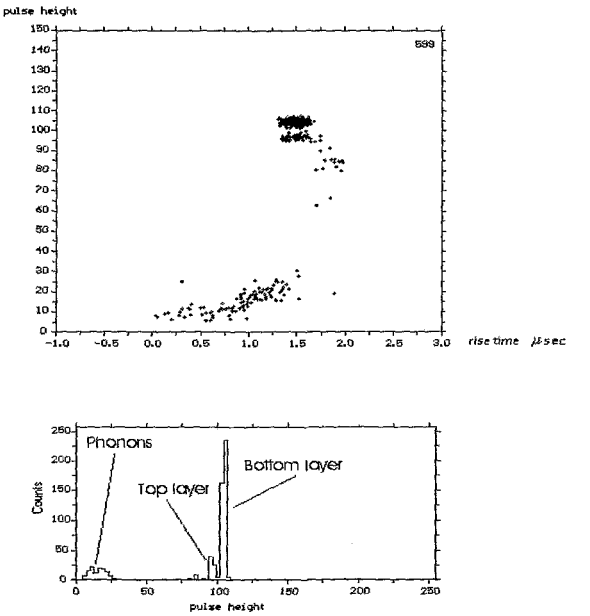

Figure 6.1: X-ray spectrum obtained with tantalum STJ. At low energy we have a phonon peak given by X-ray impacts in the absorber and at higher energy X-ray impacts in the top layer, the epitaxial layer correspond to the highest energy. For molecules measurements only energy at the top layer is important because of molecules impact occurs only in the top film.

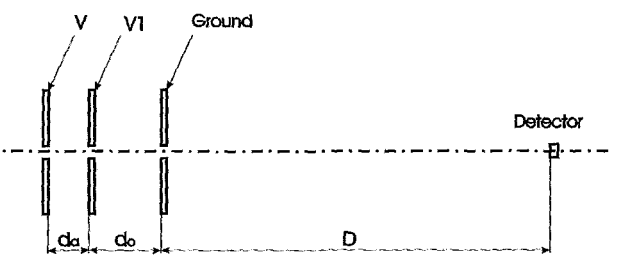

Figure 6.2: Layout of our mass spectrometer.

6.1 Comparison of detection efficiency between a classical detector and cryodetectors

It is known that the detection efficiency for an ionizing detector decreases when the molecules velocity decreases [52]. The figure 6.6 p.60 is obtained by computing the integral of the PEG peaks (see Zenobi figure 6.3 a) as a function of the velocity of the mass of molecule.
An exponential is fitted across the different points making the hypothesis that for zero mass the detection efficiency is 100%.
Cryodetectors spectrum illustrated in figure 6.3 b) showing the PEG 6'000 Da and PEG 35'000 Da are also included in the plot. The PEG 6'000 Da ionizing detector signal strength (figure 6.3 c)) is fixed on the exponential and we can note that the signal strength of the PEG 35'000 Da ionizing detector is in accordance with the projected relative signal strength.
The spectrum of figure 6.4 p.58 with four equimolar proteins has also been

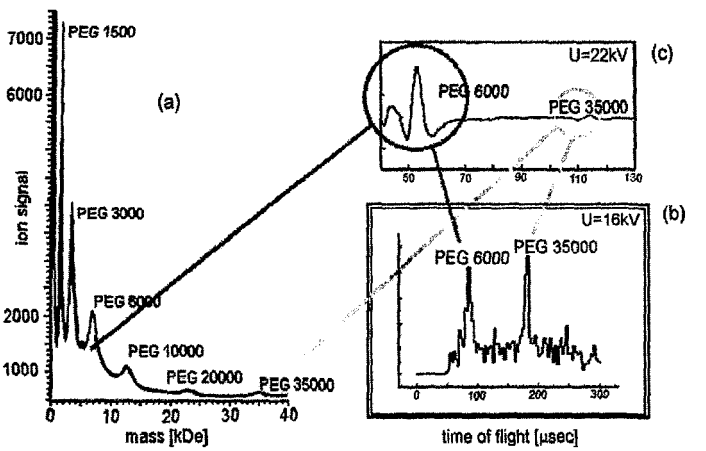

Figure 6.3: a) Equimolar spectrum of PEG from Prof. Zenobi et al. ETH, Zurich. b) Histogram obtained from an equimolar sample of PEG 6'000 Da and PEG 35'000 Da. c) Same spectrum obtained with a classical detector.

included. The insulin peak has been fixed to the exponential curve.

The results from the Lawrence Livermore National Laboratory / Lawrence

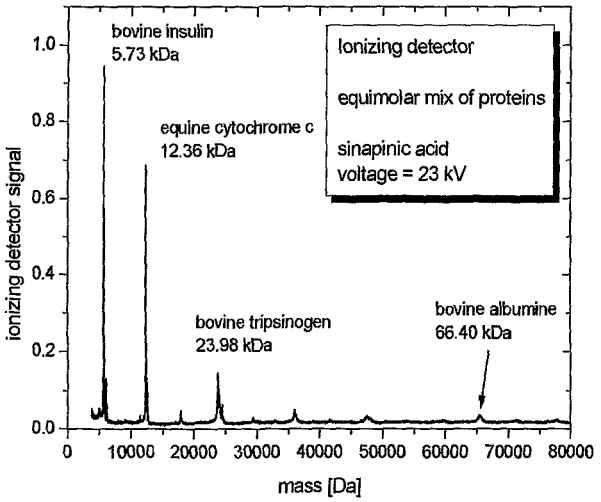

Figure 6.4: Mass spectrum of four equimolar (1 pmol) proteins in sinapinic acid (10 nmol) obtained in a MALDI-TOF mass spectrometer equipped with a conventional microchannel plate detector.

Berkeley National Laboratory group have the same tendency than the exponential fit [53].
Finally, the relative signal strength of single and double charged IgG molecules (see figure 6.5 p.59) has been added to the figure 6.6.

Therefore, we have shown that the signal strength in a conventional detector decreases hugely when the molecules velocity decreases or, in other words when the mass increases. The datas used for the model are consistent with an exponential fit. In contrast, the cryodetectors have a mass independent detection efficiency due to the calorimetric nature of the mechanism.

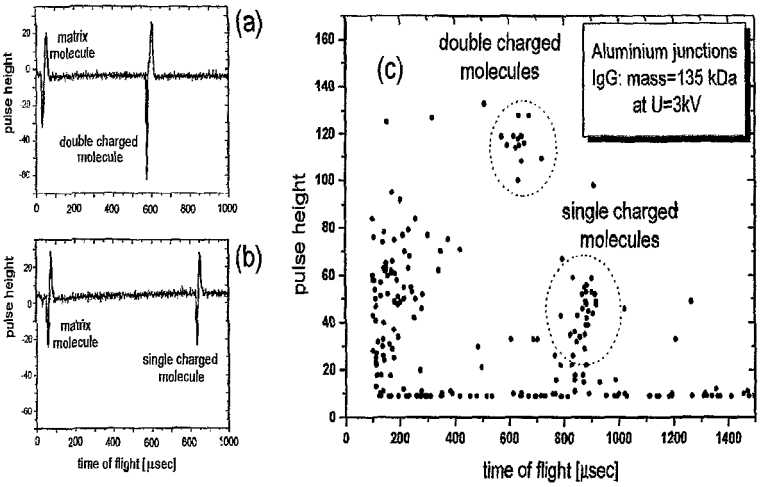

Figure 6.5: IgG pulses obtained with aluminium STJ at 3 kV a) doubly charged IgG and b) singly charged IgG. In figure c), the charge state separation given by the ions pulse height.

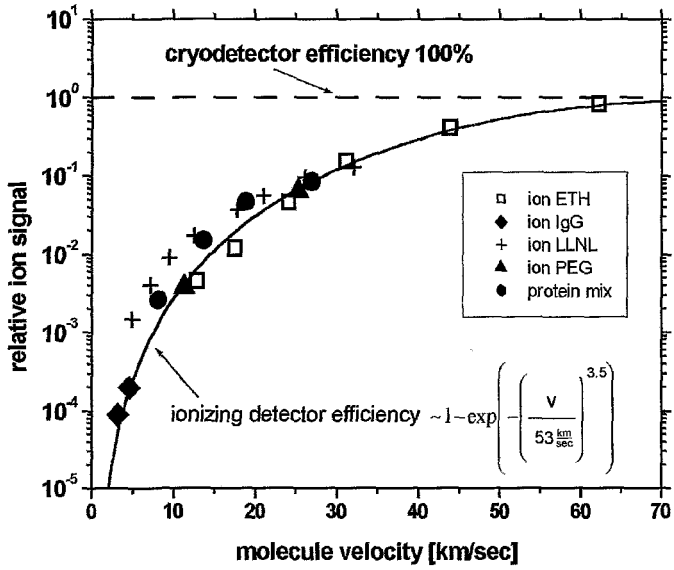

Figure 6.6: The relative signal strength of conventional ionizing detector as a function of molecule velocity as deduced from our experimental results by comparing MALDI-TOF mass spectra obtained from both ionizing detectors and cryodetectors.

6.2 Cryodetectors used for the detection of macromolecules

In this section, we are going to understand the key role of fragmentation and neutral molecules. As we will see, cryodetectors are a very powerful tool for this context.
Each neutral or charged molecules hitting the cryodetector induces a measurable signal in it, and we will see the particularity of cryodetectors to separate the molecule charge state.

Cryodetectors were mounted in a dilution fridge and kept at 80 mK during the run.

6.2.1 Time-of-flight spectrum cleaned by pulse height selection of 40-mers oligonucleotides

The first spectrum shows the detection of 40-mers oligonucleotides. The sample is prepared as follows:
1.5 μl of diamonnium citrate (0.1M) is added to an aliquot of 5 μl of 40-mers then 4 μl of ACN (50%) and 21 μl of matrix (3-HPA 10 mg/ml) are mixed together. A droplet of 3 μl is dried on the sample holder, the final concentration of oligonucleotides is 14 pmol.
A negative voltage of 8 kV is applied on the lenses. The spectrum is obtained without delayed extraction (see figure 6.7 p.62).
In order to clean the spectrum a pulse height selection can be effectuated due to the microcalorimeter nature of the cryogenic detector.
The frame illustrated in the scatter plot (figure 6.7) represents the molecules reaching the detector with an energy of 8 kV. The background molecules given by the fragmentation can be avoided. The time-of-flight selection pulse height is represented in figure 6.8.

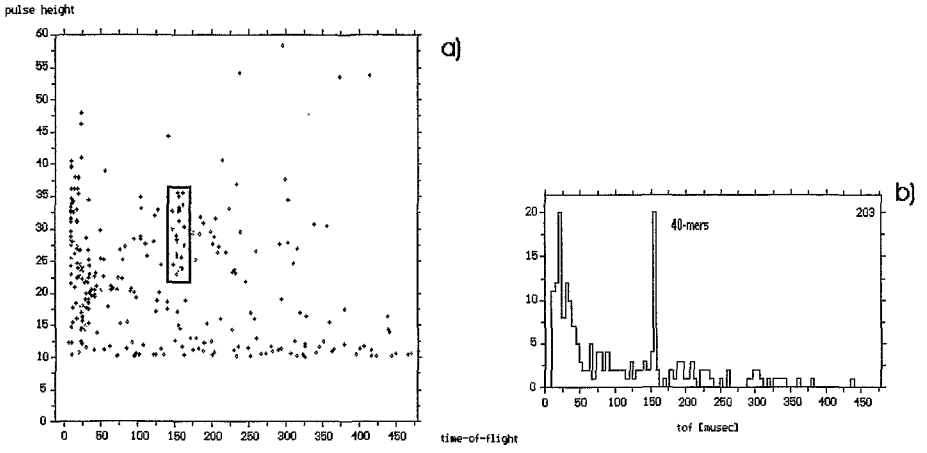

Figure 6.7: a) Scatter plot of 40-mers obtained at -8 kV with a concentration of 14 pmol on the sample holder. b) Time-of-flight histogram. No pulse height selection has been effectuated for this spectrum.

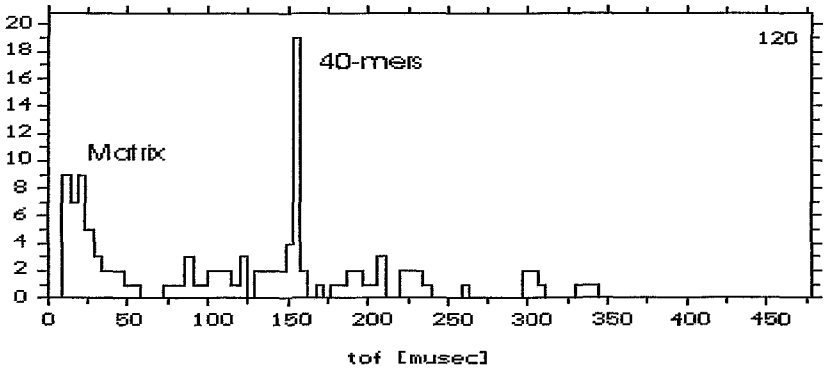

Figure 6.8: Time-of-flight selected spectrum obtained by the frame illustrated in the scatter plot on figure 6.7

6.2.2 Charge state separation in BSA

A very interesting characteristic of STJ is the ion charge state separation, classical detector being not able to do this.
BSA spectrum is used to show this behaviour. To obtain different ion charge states, a BSA sample with high concentration (90 pmol) has been used for this purpose. The laser fluence has been adjusted a little bit above the threshold.
The sample preparation is as follows: BSA has been prepared (1 mg/ml) in TFA 0.1%, $5\mu l$ of BSA is diluted in $10\mu l$ of water. The matrix used is sinapinic acid (10 mg/ml), $10\mu l$ of BSA and $10\mu l$ of matrix are mixed together. $3\mu l$ of this solution is dried on nitrocellulose blotting membrane (2 mm x 2 mm).

The high voltage applied on the electrode is 3 kV. The scatter plot obtained is illustrated on figure 6.9 p.64.

A gap between the singly charge and doubly charge is clearly demonstrated in this scatter plot. It is even possible to distinguish molecules cluster by looking their time-of-flight.

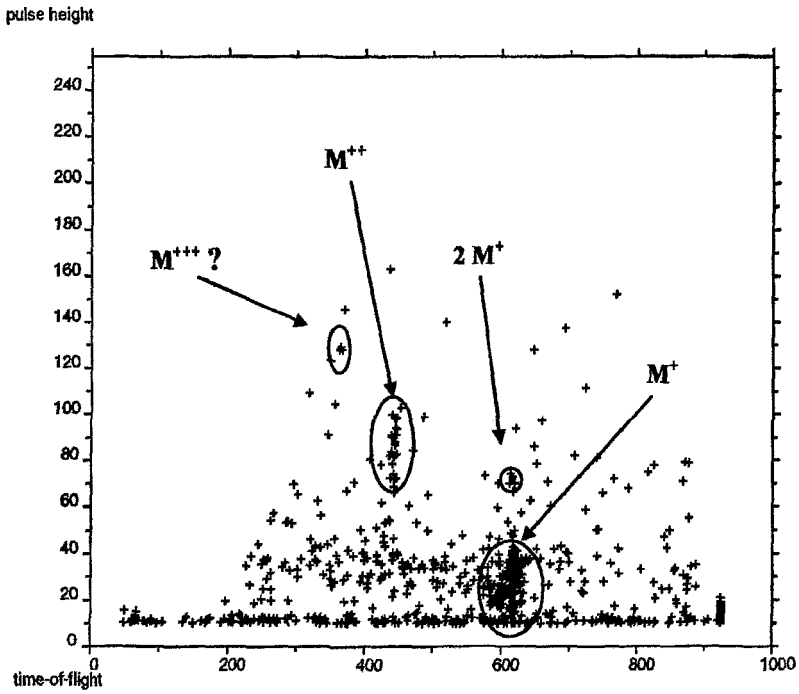

Figure 6.9: BSA scatter plot obtained at 3 kV. Ions reaching the detector with an energy of 3 keV are represented by M^+ cluster, just above a group with the same time-of-flight than M^+ but with double pulse height (6 keV) is attributed to double masses $2M^+$ hitting the detectors at the same time but at different places. Doubly charged ions have a pulse height of 6 keV but their time-of-flight is shorter than M^+ by a factor $\sqrt{2}$.

6.2.3 Characterization of polystyrene 2000 Da by Tantalum STJ

Two tantalum STJs (see section 5.2) are used as detectors, respectively 50 μm and 100 μm.
To perform the characterization of PS 2000 the sample has been prepared as follows:

- 10 mg of polystyrene 2000 are dissolved in 1 ml of tetrahydrofurane (THF).
- Dithranol (1,8,9-Anthracenetriol) is used as matrix: 10 mg of dithranol are dissolved in 1 ml of THF.
- A solution of Silver Trifluoroacetate (TFAr) is used for cationization 100 mg/ml.

The mixture among the elements is: (Matrix; PS; Salt)=(8: 1: 1), $3\mu l$ are dried on the sample holder.
Spectrum has been obtained at 12 kV with low laser fluence, the figure 6.10 p.66 shows the scatter plot of PS 2000 as well as a zoom in the interesting zone. The equivalent histogram is shown in figure 6.11 p.67.

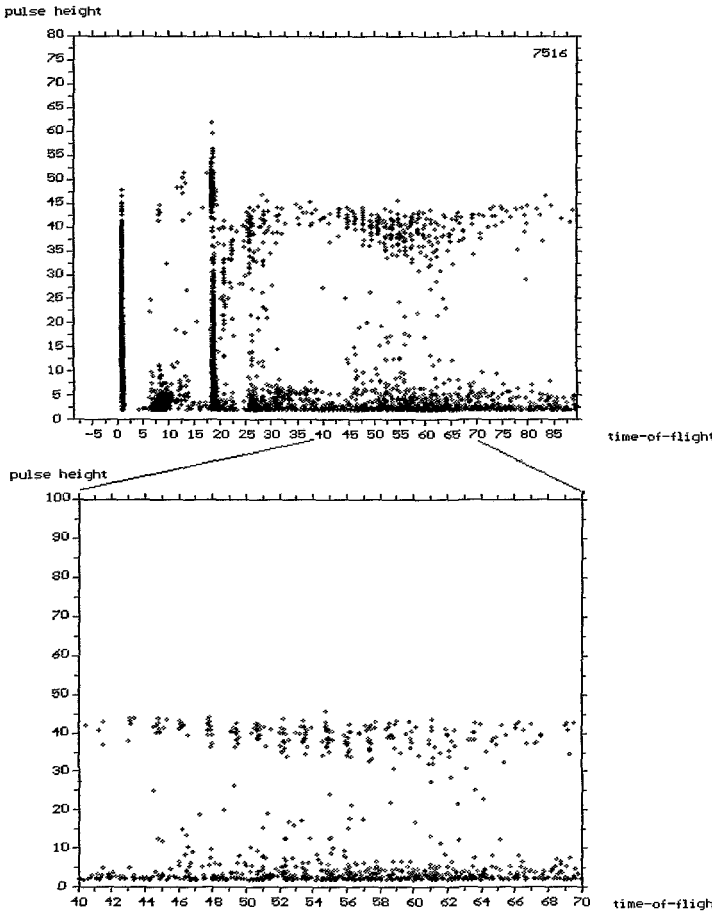

Figure 6.10: Scatter plot of polystyrene 2000 Da obtained with cryodetectors. The distribution of styrenes are clearly separated on the zoom.

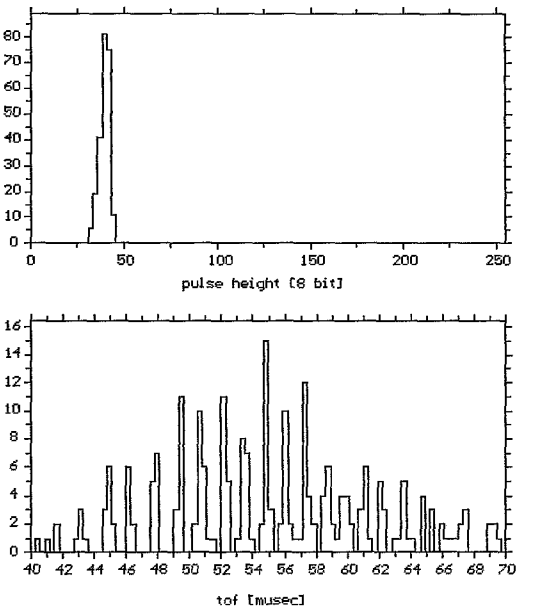

Figure 6.11: Histogram of the interesting zone. Only events with a pulse height (see figure 6.10) between 30 and 50 are recorded on the spectrum.

For the determination of accurate masses in MALDI spectra of synthetic polymer, the histogram is transformed with ORIGIN program.

For the characterization we will determine the following parameters:

- M_p, most probable peak
- M_n, the number-average molecular weight: $M_n = \Sigma n_i M_i / \Sigma n_i$
- M_w, the weight-average molecular weight: $M_w = \Sigma n_i M_i^2 / \Sigma n_i M_i$
- PD, the polydispersity calculated as M_w/M_n

where n_i represents the number of oligomer molecules having a mass M_i, therefore n_i is equivalent to calculating the integral of each peak representing a mass M_i.
Values obtained with our system are resumed on table below as well as gel permeation chromatography values given by the manufacturer FLUKA.

MALDI				GPC			
M_p	M_n	M_w	PD	M_p	M_n	M_w	PD
2084	2152	2230	1.04	1920	1790	1900	1.06

This shows that cryodetectors can be used for the characterization of synthetic polymers. In this example the study of the end group has not been done because the resolution is not sufficient to distinguish the terminations. Contrary to the classical detectors where the signal due to the higher masses are often too weak and is therefore lost in the baseline noise, cryodetectors can be the solution to this MALDI-TOF problem.
PS 2000 Da spectra will be retake in the next section 6.2.4 for the study of the relation between the laser fluence and fragmentation.

6.2.4 High efficiency detection of neutral molecules and fragments

The detection of neutral molecules has been performed with aluminium STJ detectors for insulin measurements and tantalum STJ for polystyrene detection. Some results on the neutral and ion yields can be obtained with MALD/PI (Matrix-Assisted Laser Desorption/ Photon Ionization) [58].
Due to the microcalorimeter nature of the cryodetectors, there is no difference between the ions or neutrals molecules detection because the STJ are sensitive to the total energy deposited into the detectors.
To detect the neutral molecules, deflection plates are used as illustrated on figure 6.12.

In order to illustrate this principle, some measurements have been carried

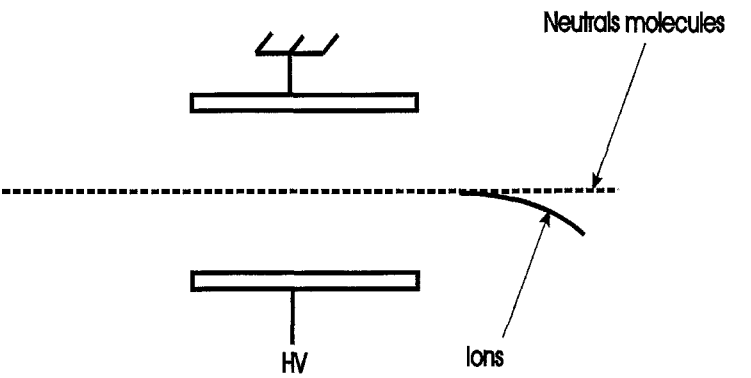

Figure 6.12: Schematic drawing of the ions deviation by deflection plates.

out with insulin and polysterene 2000 Da.

- **Measurements effectuated with insulin (5735 Da) and aluminium junction**

On the figure 6.13 a), we can see the scatter plot of an insulin sample, these spectra has been obtained without deflection plates. To perform a scatter

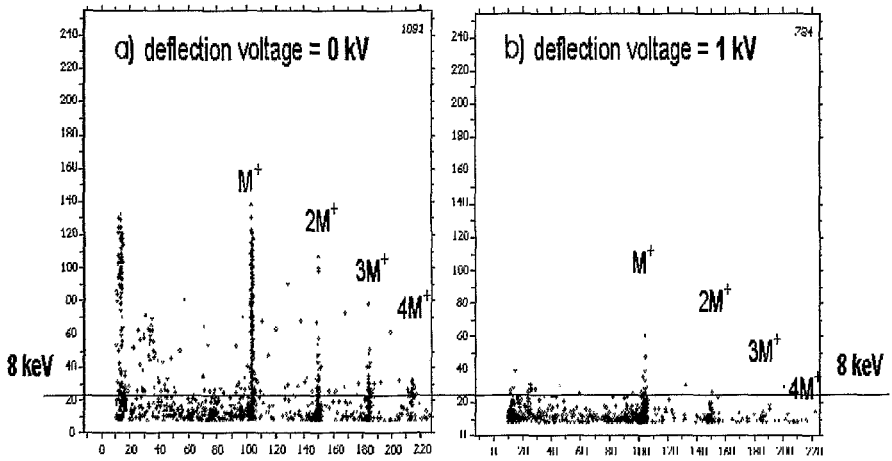

Figure 6.13: Scatter plots of an insulin sample at 8 kV and **high laser fluence**. a) No deflection plate used during the measure, charged and neutral molecules can reach the detector. b) Deflection plate is kept to 1 kV during the measure, only neutral molecules and neutral fragments can reach the detector

plot of neutral molecules, the deflection plate is kept at 1 kV during the measurement (see figure 6.13 b).
To look at the effect of the laser on the fragmentation, the experiment has been carried out with reduced fluence laser. The result is illustrated in figure 6.14 a) p.71.

Clearly, we can see less background molecules in figure 6.14 b) due to the fact that laser energy is relaxed in the matrix and therefore create more excited ions fragmenting during the acceleration.

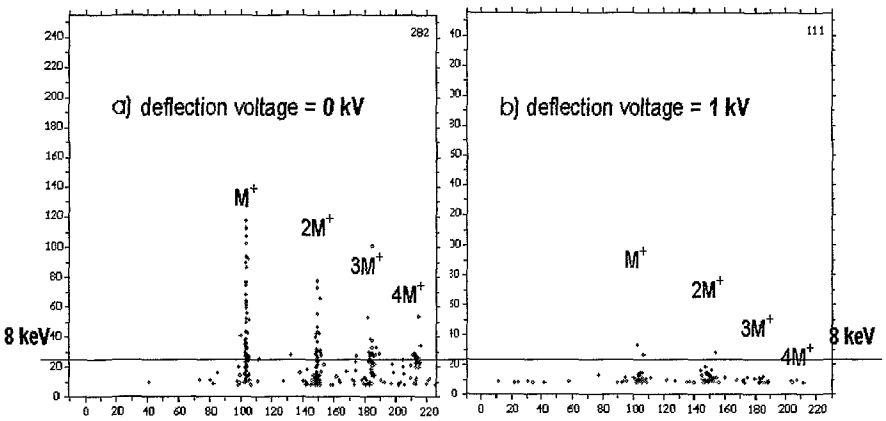

Figure 6.14: Scatter plot of an insulin sample at 8 kV and **low laser fluence**. a) No deflection plate used during the measure, charged and neutral molecules can reach the detector. b) Deflection plate is kept to 1 kV during the measure, only neutral molecules and neutral fragments can reach the detector

- **Measurements performed with polystyrene 2000 Da and tantalum junction**

The recipe used for PS 2000 Da has been already described in section 6.2.3 . The first scatter plot as well as the histogram is obtained with high fluence laser. Background due to the molecules fragments is clearly shown on scatter plot (figure 6.15). For comparison, we have took from the same sample a spectrum at the threshold fluence laser (see figure 6.16 p.73). With this

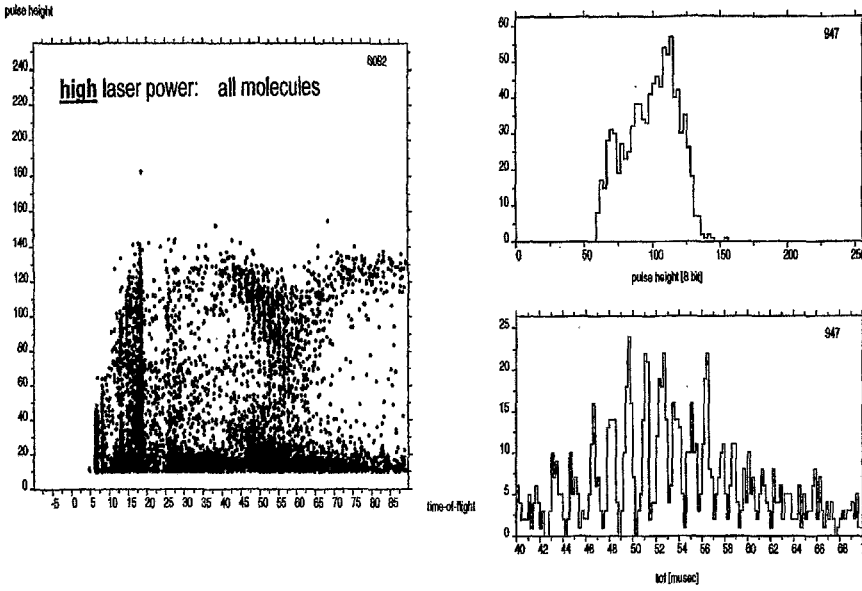

Figure 6.15: Scatter plot of polystyrene 2000 Da with high laser fluence and its corresponding time-of-flight histogram.

spectrum we can see clearly that there is less fragmentation with low power laser, only molecules with a pulse height corresponding to 12 kev reached the detector.

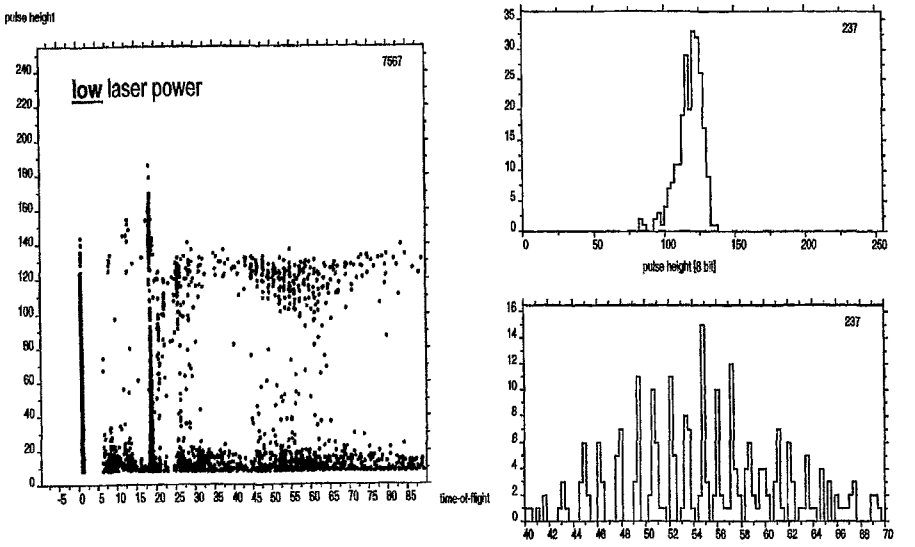

Figure 6.16: Scatter plot of polystyrene 2000 Da at threshold laser fluence and its corresponding time-of-flight histogram.

The last spectrum has been effectuated with a voltage of 1 kV applied on deflection plate. The laser fluence was adjusted above the threshold (see figure 6.17). A structure at the right time-of-flight is given by the neutral

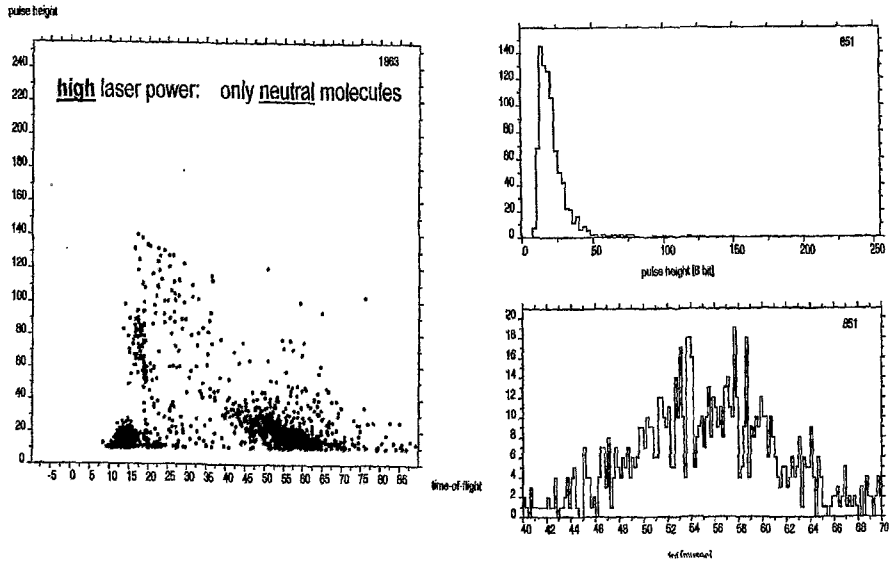

Figure 6.17: Scatter plot of polystyrene 2000 Da showing only neutral molecules reaching the detector

molecules. No polystyrene structure appears in time-of-flight histogram.

In conclusion, the detection of neutral molecules and neutral fragments is very effective with cryodetectors. In addition, they are allow as to understand better the relation between the laser fluence and the fragmentation. As we have already said the fragments are the signature of the whole molecules and therefore cryodetectors can be a useful tool in the *Proteomics project.*

6.3 Special characteristics obtained with cryodetectors

In this section, we will show some characteristics obtained with different kinds of cryodetectors. For example, we will point out the fact that cryodetectors do not need high voltage acceleration or the high sensivity measurement done with oligonucleotides.

6.3.1 IgG beam profile at 3 kV

IgG has been prepared (1 mg/ml) in TFA 0.1%. The matrix used is sinapinic acid (10 mg/ml), the concentration of IgG on sample holder is 15 pmol.

The voltage on the first electrode is 3 kV and 2.8 kV on the second one, einzel lens voltage is kept at 1.4 kV. With this weak electric field and our time-of-flight distance to the detector, the IgG reaches the detector after almost 1 ms.
Array of aluminium junctions used in this measure is illustrated in figure 6.18.

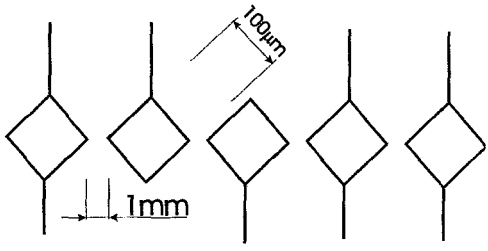

Figure 6.18: Array of five aluminium junctions.

The diverse IgG spectra obtained with the cryodetectors are shown in figure 6.19 p.76.
Nevertheless, the array of junctions is very useful to increase the detection area without degrading the signal-to-noise ratio.
Junctions array is exploited to obtain some information about the beam profile as illustrated in figure 6.19.
Excepted the fact which is remarkable to obtain a IgG spectrum at 3 kV, we can see gaussian profile of molecules beam.

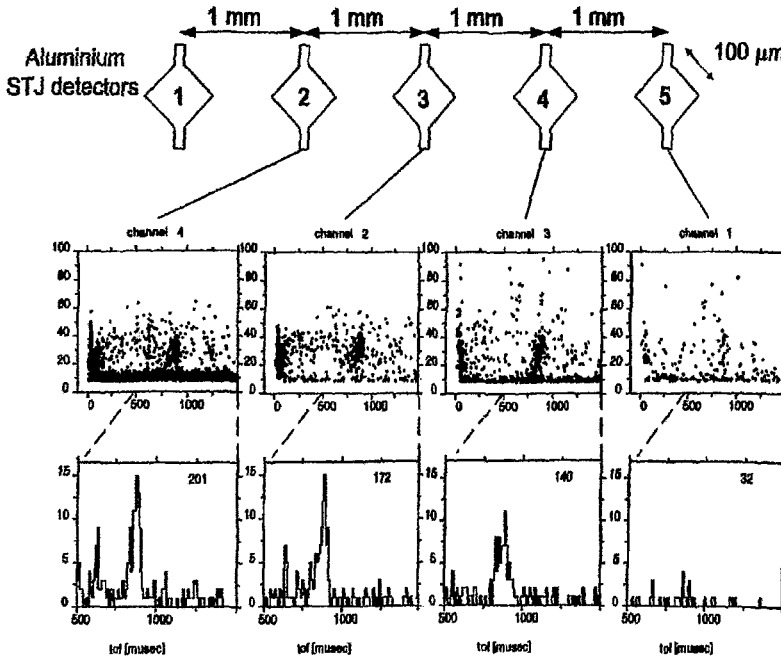

Figure 6.19: IgG beam profile obtained with an array of five aluminium junctions.

6.3.2 Behavior of tantalum strips upon molecules impact

A tantalum strip possesses a junction at both extremities and therefore a particle induces two signals for the same event. Both signals have different rise times, pulse heights and decay times (see figure 4.14 p.43) given by the fact that events are closer to one junction than to the other one. Only events in the middle of the strip have the same shape.

A polystyrene spectrum obtained with tantalum strip is illustrated in figure 6.20. The recipe for the sample preparation has already been explained in section 6.2.3.
The voltage acceleration is 10 kV and the second one has been adjusted at 7.1 kV, no einzel lens was used for this measurement.
An event created close to a junction induce a pulse with a fast rise time

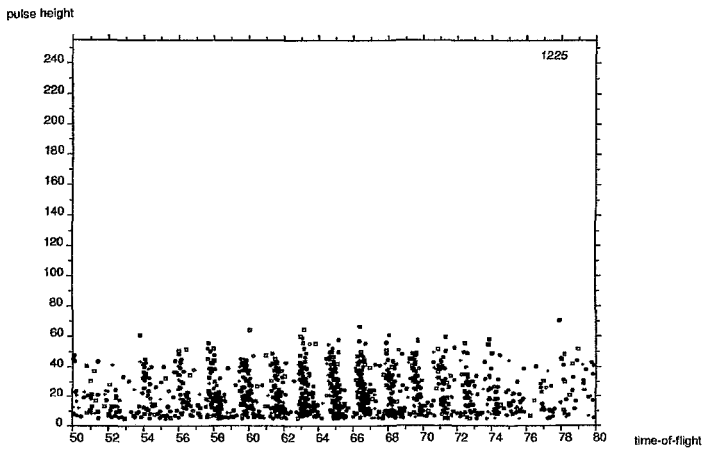

Figure 6.20: Scatter plot of PS 2000 obtained at 10 kV with tantalum strips. Monomer peaks are slightly tilted due to the fact that a molecule hitting the absorber close to one of the STJ gives large pulses with fast rise time and the signal received by the other STJ is a small pulse with a long rise time. The time for quasiparticle diffusion in the absorber from molecule events between the two STJ takes about 1 μs.

whereas in the other junction, the pulse has a longer rise time. This fact can

be explained by the quasiparticle diffusion time in tantalum strips being not the same for each junction.

6.3.3 Equimolar mixture of polyethylene glycol (PEG)

As we have already said, MALDI-TOF technique is a very important tool for the polymers characterization.

In order to demonstrate the power of the cryodetectors, a mixture of equimolar polyethylene glycols has been prepared.
Two aluminium STJ with $100\mu m$ x $100\mu m$ area are used as cryodetectors.

A concentration of 50 picomoles of each PEG(4000 Da; 8000 Da; 12'000 Da; 20'000 Da; 35'000 Da) are mixed together. The matrix used is 2.5-dihydroxybenzoic (mass =154 Da) at the concentration 100 mg/ml dissolved in water and ethanol (9:1 V:V). A cationizating agent as NaCl 0.1M is added to the mixture.
The sample is prepared as follows:
100 μl of each PEG are mixed together, 25 μl of NaCl and 525 μl are added to the mixture; then 3 μl of the substance is dried on the sample holder. The ratio between the matrix and the analyte is $\frac{M}{A} = 1500$.

The group of Prof. Zenobi at the ETH in Zurich provided us their data showing their measures obtained with a microchannel plate at 30 kV (figure 6.21 p.80, this figure has been already shown in section 6.1.). This spectrum demonstrates clearly that sensivity decreases quickly for the massive molecules. Our measurements with the aluminium junctions have been recorded at 8 kV according to the recipe described above.
The raw spectra of a equimolar PEG are shown in figure 6.22 p.80. The gaussian plot on the spectrum is certainly due to the charged and neutral fragments and neutral whole molecules. The subtraction of the background from the spectrum is carried out to obtain a clean spectrum as illustrated in figure 6.23 a) p.81.
The figure 6.23 b) compares the detection efficiency between a classical detector and cryodetectors at 8 kV. The errors plotted in the figure 6.23 b) are due to the Poisson statistics.
The question concerning the detection efficiency has been developed in details in section 6.1.

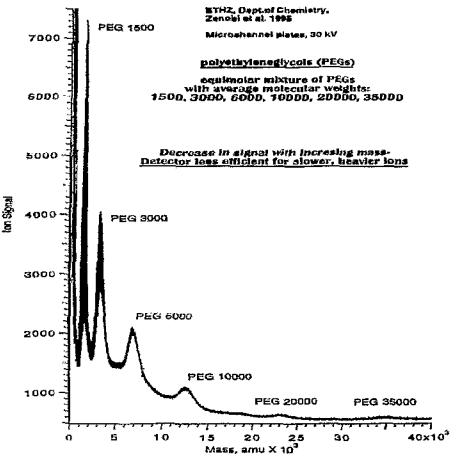

Figure 6.21: Ionizing detector signal from a microchannel plate at 30 kV for an equimolar mixture of polyethylene glycol. [Courtesy of Prof. Zenobi]

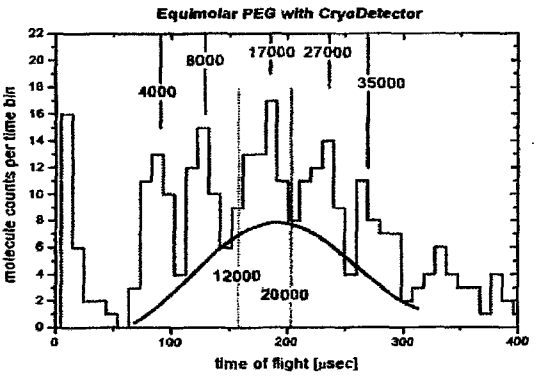

Figure 6.22: Raw data of equimolar PEG obtained with the cryodetectors at 8 kV. The most probable molecular weight M_p for the PEG 12'000 Da and 20'000 Da has been measured respectively as a PEG 17'000 Da and PEG 27'000 Da. The theoretical positions of PEG 12'000 Da and PEG 20'000 Da are shown by dashed straightline.

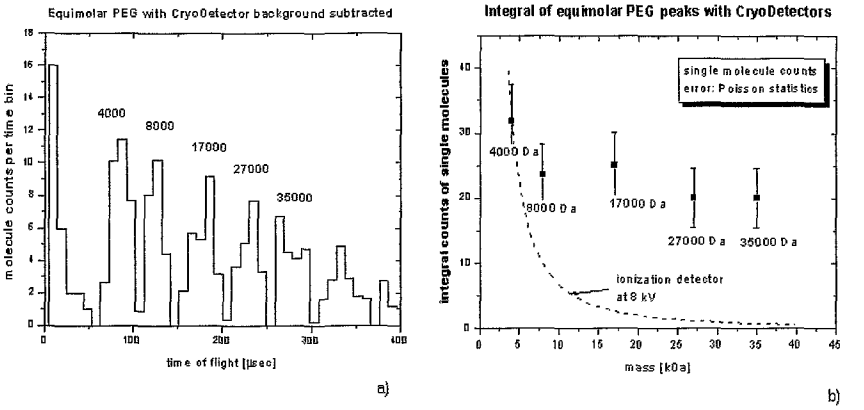

Figure 6.23: a) Spectrum obtained after background subtraction. The number of molecules counts per time bin decreases when the mass of molecule increases: this effect can be explained by the fact that bigger molecules can break up more easily than small molecules. b) To point out the detection efficiency of cryodetectors independently, the integral of each peak is computed in function of the most probable molecular weight.

6.3.4 Equimolar measurement of oligonucleotides

Two aluminium STJ $100\mu m$ x $100\mu m$ area each are used as cryodetector for this experiment. The acceleration voltage is 8 kV and the second one is 6.9 kV.

A measurement with four equimolar oligonucleotides 40-mers, 70-mers, 100-mers and 120-mers has been performed with a final concentration of **8 pmol** for each oligonucleotide.
As the oligonucleotides can often split up themselves, all the more if the chains are very big as 100-mers or 120-mers. To get out informations from the raw data shown in figure 6.24, some manipulations are necessary.
A refined analysis is necessary to extract the signal molecules hidden in this

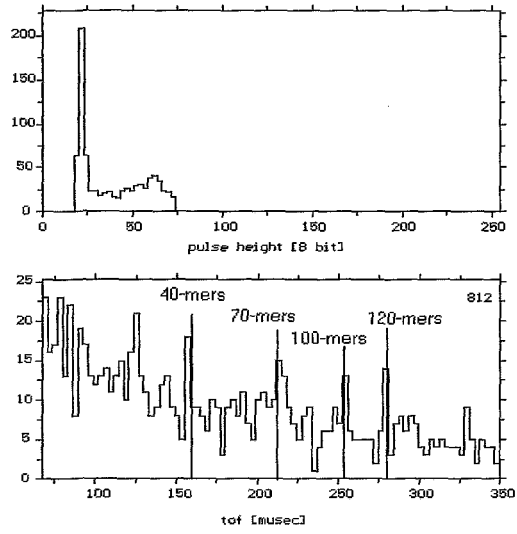

Figure 6.24: Equimolar sample (8 pmol) of four oligonucleotides obtained at 8 kV. The straight lines represent the theoritical positions of the four oligonucleotides.

spectrum.
First, we take only the laser shots with events in one of the four predicted

oligonucleotides positions and having pulse height between 50 and 80. This pulse height selection corresponds to 8 keV and intact oligonucleotides, the result is shown in figure 6.25 a). In figure 6.25 b) only pulse height between 20 and 50 is illustrated. This pulse height does not correspond to 8 keV and the most probable explanation are fragments and neutral molecules.

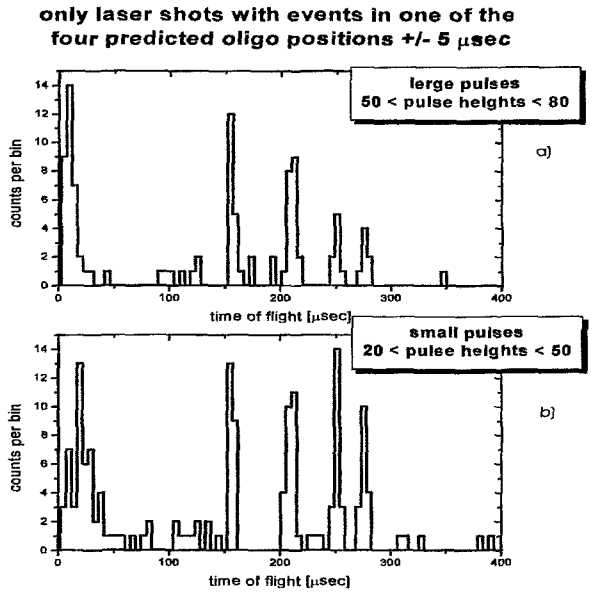

Figure 6.25: Selection peaks corresponding to the four oligonucleotides positions a) represent the intact molecules having 8 keV, b) small pulses certainly due to the fragmentation.

As we can observe in figure 6.25 a), the number of counts per bin decreases for the massive oligonucleotides. This can be explained by the fact that longer chains are easier to break than the shorter ones; therefore fragmentation is proportional to the length of oligonucleotides. In figure 6.25 b), the number of counts per bin is roughly the same.

Even if the spectrum shown in figure 6.24 is not striking, we can put forward that we have seen molecules in each position of the four equimolar oligonucleotides at 8 pmol concentration.

6.4 High resolution measurement with cryo-detectors

6.4.1 Time resolution on IgG obtained with tantalum strips

Even if the quasiparticles have to travel in absorber before inducing a signal in the junctions, we will see that this kind of detector can be used for high resolution measurements.

On figure 6.26 an IgG scatter plot is shown as well as the hot spot selection. The recipe for the IgG sample is the same one than described in section 6.3.1. The time-of-flight histogram corresponding to the full scatter plot is shown in

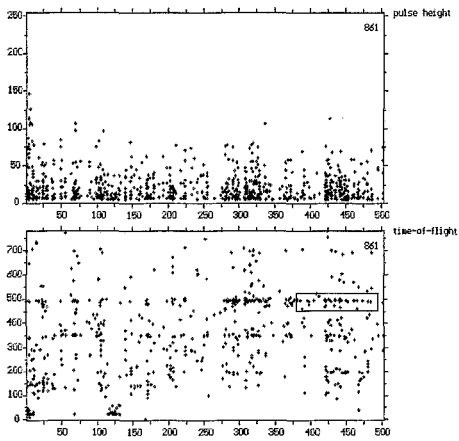

Figure 6.26: Scatter plot of IgG at 12 kV. The frame represents the hot spot on the sample.

figure 6.27 p.85. The pulses selection on the scatter plot (figure 6.26) gives a time-of-flight histogram with a better time resolution (see figure 6.28). The time-of-flight resolution obtained from the histogram is $t/\Delta t = 140$. This time-of-flight has been obtained without delay extraction.
Sometimes a layer of blotting nitrocellulose on the sample holder can improve the signal-to-noise ratio.

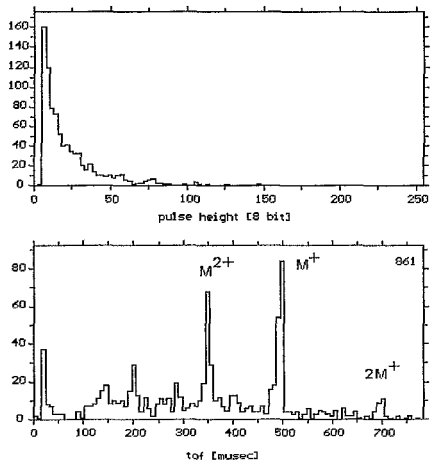

Figure 6.27: Time-of-flight histogram of IgG at 12 kV without selection pulse.

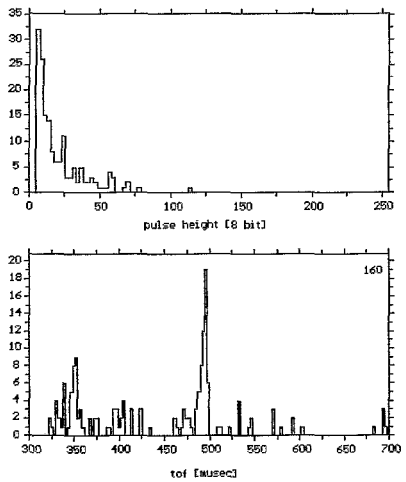

Figure 6.28: Time-of-flight histogram of IgG at 12 kV with selected pulses (the frame on figure 6.26. The time per bin is $2\mu s$)

Chapter 7

Conclusions

One of the most important characteristics of the cryodetectors is certainly the 100% detection efficiency for macromolecules. This is very important for the detection of high mass heavier than 100 kDa. For these masses, the peak intensity obtained from a classical detector is reduced by a factor 10'000.

Due to the calorimetric nature of our cryogenic detectors, we have shown the ability to separate the charge state of ions. Maybe this characteristic could help to understand better the ionization principle.

Characterization of synthetic polymers can easily be performed with cryodetectors. The problem with the synthetic polymers characterization is the same one as with classical detectors: namely the sample quality. The solution is to make good polymers samples with new matrices, new salts,... . The sample preparation becomes crucial particularly for the detection of high masses.

With cryodetectors, fragmentation process and neutral molecules can be studied with more accuracy. The scatter plot (pulse height versus time-of-flight) is a useful tool for a comprehensive study of fragmentation which can occur in different parts of the mass spectrometer. The peak shape obtained has every information about what happens during the time of flight.

High sensitivity measurements are very easy to perform because of the single molecule counting process. Efforts have to be made on the mass spectrometer geometry to get around the small size detectors problem.

Strip detectors are an elegant solution if they can be extended to $800\mu m$ and work with 8 strips (16 junctions).

For the moment, charge state separation with strip detectors has not been resolved. We are working on a new electronic box based on a other charge preamplifier (Amptek 225). Another interesting characteristic of the strip is the fact to know the position on the strip where the molecule has deposited its energy.
STJ arrays are also a good device to increase the detection area keeping the particularity to obtain some information about the molecules beam as demonstrated in section 6.3.1.

Mass resolution is not limited by cryogenic detectors but by the same problems encountered with classical method. Spatial dispersion and velocity dispersion are the limiting factors. Solutions are provided by delayed extraction and reflectron.

Liquid MALDI is currently tested to desorb molecules from liquid matrix such as glycerol, 3-NBA,... using infrared laser CO_2 at $10.6\mu m$ wavelength.

Bibliography

[1] M. Barber, R.S Bordoli, R.D Sedgewick and A.N Tyler, *Atom Bombardement of Solids (FAB): A new source for mass spectrometry.* J. Chem. Soc. Chem. Commun. (1981) 325.

[2] A. Bennighoven and W.K Sichtermann, *Detection, Identification and Structural Investigation of Biologically Important Compounds by Secondary Ion Mass Spectrometry.* Anal.Chem. **50** (1978) 1180.

[3] M. Karas and F. Hillenkamp, *Matrix-assisted ultraviolet laser desorption of non-volatile compounds.* Int. J. Mass. Spectrom. Ion. Proc. **78** (1987) 53.

[4] K. Tanaka, H. Waki, Y. Ido, S. Akita and T. Yoshida, *Protein and Polymer Analysis up to m/z 100'000 by Laser Ionization Time-of-Flight Mass Spectrometry.* Rapid Commun. Mass. Spectrom. **2** (1988) 151.

[5] D. Twerenbold; *Biopolymer mass spectrometer with crayogenic particle detectors.* Proceedings of the fifth wokshop on *Low temperature Detectors*.eds H.R. Ott and A. Zehnder, Nucl.Instr. and Meth. A **370** (1996).

[6] M.A Claydon, S. Davey, V. Edwards-Jones and D.B Gordon, *The rapid identification of intact microorganisms using mass spectrometry.* Nature Biotechnology **14** (1996) 1584.

[7] A. Lapolla, D. Fedele, R. Aronica, M. Garbeglio, M. D'Alpaos, R. Seraglia and P. Traldi, *Evaluation of IgG Glycation Levels by Matrix-assisted Laser Desorption/Ionization Mass Spectrometry* Rapid Commun. Mass Spectrom. **11** (1997) 1342.

[8] R.D Holland, J.G Wilkes, F. Rafii, J.B Sutherland, C.C Persons, K.J Voorhees and J.O Lay, *Rapid Identitification of Intact Whole Bacteria Based on Spectral Patterns using Matrix-assisted Laser Desorp-*

tion/Ionization with Time-of-Flight Mass Spectrometry. Rapid. Commun. Mass. Spectrom **10** (1996) 1227.

[9] A. Westman, C.L Nilsson and R. Ekman, *Matrix-assisted Laser Desorption/Ionization Time-of-Flight Mass Spectrometry Analysis of Proteins in Human Cerebrospinal Fluid.* Rapid. Commun. Mass. Spectrom **12** (1998) 1092.

[10] R.E March, R.J Hughes and J.T Todd, *Quadrupole Storage Mass Spectrometry* **102** Chemical Analysis, Wiley (1989).

[11] R.J Cotter ed.; *Time-of-Flight Mass Spectrometry.* ACS symposium series **549**, American Chemical Society, Washington DC, (1994).

[12] F.J Vastola, R.O. Mumma and A.J Pirone, *titre* Org. Mass. Spectrom. **3** (1970) 101.

[13] J. Krause, M. Stoeckli and U.P Schlunegger, *Studies on the Selection of New Matrix for Ultraviolet Matrix-assisted Laser Desorption/Ionization Time-of-Flight Mass Spectrometry.* Rapid. Commun. in Mass Spectrom. **10** (1996) 1927.

[14] M.V Buchanan and R.L Hettich, *Fourier Transform Mass Spectometry of High-Mass Boimolecules.* Anal. Chem. **65** (1993) 245.

[15] S. Niu, W. Zhang and B.T Chait, *Direct Comparaison of Infrared and Ultraviolet Wavelenght Matrix-assisted Laser Desorption/Ionization Time-of-Flight Mass Spectrometry of Proteins.* J. Am. Soc. Mass. Spectrom. **9** (1998) 1.

[16] S. Berkenkamp, C. Menzel, M. Karas and F. Hillenkamp, *Performance of Infrared Matrix-assisted Laser Desorption/Ionization Time-of-Flight Mass Spectrometry with Laser Emitting in the 3μm Wavelenth Range.* Rapid. Commun. in Mass Spectrom. **11** (1997) 1399.

[17] K.L Caldwell and K.K Murray, *Mid-Infrared Matrix-assisted Laser Desorption/Ionization with a Water/Glycerol Matrix.* Appl. Surf. Sc. **127-129** (1998) 242.

[18] R. Knochenmuss, F. Dubois, M.J Dale and R. Zenobi, *The Matrix Suppression Effect and Ionization Mechanisms in Matrix-assisted Laser Desorption/Ionization.* Rapid. Commun. in Mass Spectrom. **10** (1996) 871.

[19] A. Overberg, M. Karas and F. Hillenkamp, *Matrix-assisted Laser Desorption/Ionization of Large Biomolecules with a TEA-CO_2 Laser.* Rapid. Commun. in Mass Spectrom. **5** (1991) 129.

[20] R.C Beavis and B.T Chait, *Cinnamic Acid Derivatives as Matrices for Ultraviolet Laser Desorption Mass Spectrometry of Proteins.* Rapid. Commun. in Mass Spectrom. **3** (1989) 432.

[21] Y.F Zhu, N.I Taranenko, S.L Allman, S.A Martin, L. Haff and C.H Chen, *The Effect of Ammonium Salt by Matrix-assisted Laser Desorption/Ionization Time-of-Flight Mass Spectrometry.* Rapid. Commun. in Mass Spectrom. **10** (1996) 1591.

[22] I. Dunham, N. Shimizu, B.A Roe, S. Chissoe et al. *The DNA sequence of human chromosome 22* Nature **402** (1999) 445.

[23] B.A Mamyrin, V.I Karataev, D.V Shmikk and V.A Zagulin, *The mass reflectron, a new nonmagnetic time-of-flight mass spectrometer with high resolution.* Sov. Phys. JETP **37** (1973) 45.

[24] W.C Wiley and I.H Mc Laren, *Time-of-flight mass spectrometer with improved resolution.* Rev. Sci. Instrum. **26** (1955) 1150.

[25] J. Bai, Y.H Liu and D. Lubman, *Matrix-assisted Laser Desorption/Ionization Mass Spectrometry of Restriction Enzyme-digested Plasmid DNA Using an Active Nafion Substrate.* Rapid. Commun. in Mass Spectrom. **8** (1994) 687.

[26] P. Juhasz, M.T Roskey, I.P Smirnov, L.A Haff, M.L Vestal and S.A Martin, *Application of Delayed Extraction Matrix-assisted Laser Desorption Ionization Time-of-Flight Mass Spectrometry to Oligonucleotide Analysis.* Anal. Chem. **68** (1996) 941.

[27] M.T Roskey, P. Juhasz, I.P Smirnov, E.J Takach, S.A Martin and L.A Haff, *DNA sequencing by delayed extraction matrix-assisted laser desorption/ionization time-of-flight mass spectrometry.* Biochemistry **93** (1996) 4724.

[28] H. Kster, K. Tang, D.J Fu, A. Braun, D. van den Boom, C.L Smith, R.J Cotter and C.R Cantor, *A strategy for rapid and efficient DNA sequencing by mass spectrometry.* Nature Biotechnology **14** (1996) 1123.

[29] C.M Bentzley, M.V Johnston, B.S Larsen and S. Gutteridge, *Oligonucleotide Sequence and Composition Determined by Matrix-assisted Laser Desorption/Ionization.* Anal. Chem. **13** (1996) 2141.

[30] J. Bardeen, L.N. Cooper and J.R. Schrieffer, *Theory of Superconductivity.* Phys. Rev. **108** (1957) 1175.

[31] J.R Primack, D. Seckel and B. Sadoulet, *Detection of cosmic dark matter* Ann. Rev. Nucl. Part. Sci. **38** (1988) 751.

[32] A. Alessandrello and al., *A new search for neutinoless $\beta\beta$ decay with a thermal detector* Phys. Lett. **B335** (1994) 519.

[33] B.A Young, B. Cabrera, A.T Lee and B.L Dougherty, *Detection of elementary particles using crystal acoustic detectors with titanium edge phonon sensors.* Nucl. Instr. and Meth. **A311** (1992) 195.

[34] K.D Irwin, *An application of electrothermal feedback for high resolution cryogenic particle detection.* Appl. Phys. Lett. **66**(15) (1995) 1998.

[35] I. Giaver, *Electron tunneling between two superconductors* Phys. Rev. Lett. **5** (1960) 464.

[36] I. Giaver, *Energy gap in superconductors measured by electron tunneling* Phys. Rev. Lett. **5** (1960) 147.

[37] D. Twerenbold, *Giaver-Type Superconducting Tunneling Junction as High Resolution X-Ray detectors.* Thesis, Diss. ETH No. 8038, Zurich 1986.

[38] D. Twerenbold, *Nonequilibrium model of the superconducting tunneling X-Ray detector.* Phys. Rev. B**34** (1986) 7748.

[39] D. Gerber, *Cryogenic Detectors as High-Efficiency Detectors of Single Massive Macromolecules* Thesis, Univ. of Neuchtel 1998.

[40] Y. Gonin, *Fabrication d'un rseau de jonctions supraconductrices comme dtecteur de macromolcules et construction d'un vaporateur canon lectrons U.H.V.* Diploma work, Univ. of Neuchtel.

[41] A. Netuschill, *Detecteurs cryogeniques. Analyse d'oligonuvleotides par spectrometrie de masse MALDI-TOF.* Diploma work, Univ. of Neuchtel.

[42] F. Rossel, *Spectrometrie de masse MALDI-TOF avec un reseau de jonctions supraconductrices comme detecteur de polymeres synthetique.* Diploma work, Univ. of Neuchtel.

[43] G.C Hilton, J.M Martinis, D.A Wollmann, K.D Irwing, L.L Dulcie, D. Gerber, P.M Gillevet and D. Twerenbold, *Impact energy measurement in time-of-flight mass soectrometry with cryogenic microcalorimeter.* Nature **391** (1998) 672.

[44] D. Twerenbold, J.-L Vuilleumier, D. Gerber, A. Tadsen, B. van den Brandt and P.M Gillevet, *Detection of single macromolecules using a cryogenic particle detector coupled to a biopolymer mass spectrometer.* Appl. Phys. Lett. **68**(24) (1996) 3503.

[45] G. Montaudo, M. Montaudo, C. Puglisi, F. Samperi, *Characterization of Polymers by Matrix-assisted Laser Desorption/Ionization Time-of-Flight Mass Spectrometry: Molecular Weight Estimates in Samples of Varying Polydispersity* Rapid. Commun. in Mass Spectrom. **9** (1995) 453.

[46] G. Montaudo, E. Scamporrino, D. Vitalini, P. Mineo, *Novel Procedure for Molecular Weight Averages Measurement of Polydisperse Polymers Directly from Matrix-assisted Laser Desorption/Ionization Time-of-Flight Mass Spectra* Rapid. Commun. in Mass Spectrom. **10** (1996) 1551.

[47] J. Axelsson, E. Scrivener, D.M Haddleton and P.J Derrick, *Mass Discrimination Effects in an Ion Detector and Other Causes for Shifts in Polymer Mass Distributions Measured by Matrix-assisted Laser Desorption/Ionization Time-of-Flight Mass Spectrometry* Macromolecules **29** (1996) 8875.

[48] G. Montaudo, M. Montaudo, C. Puglisi, F. Samperi, *Characterization of Polymers by Matrix-assisted Laser Desorption/Ionization Time-of-Flight Mass Spectrometry. End Group Determination and molecular Weight Estimates in Poly(ethylene glycols).* Macromolecules **28** (1995) 4562.

[49] M.W.F Nielen and S. Malucha, *Characterization of Polydisperse Synthetic Polymers by Size-exclusion Chromatography/Matrix-assisted Laser Desorption/Ionization Time-of-Flight Mass Spectrometry.* Rapid. Commun. in Mass Spectrom. **11** (1997) 1194.

[50] C. Jackson, B.- Larsen and C. McEwen, *Comparison of Most Propable Peak Values as Measured for Polymer Distributions by MALDI Mass spectrometry and by Size Exclusion Chromatography.* Anal. Chem. **68** (1996) 1303.

[51] H.S Creel, *Prospects for the Analysis of High Molar Mass Polymers using MALDI Mass Spectrometry* TRIP Vol.1 **11** (1993) 336.

[52] D. Twerenbold, D. Gerber, D. Gritti, Y. Gonin, A. Netuschill, F. Rossel, D. Schenker and J.-L Vuilleumier, *Single molecule detector for mass spectrometry with mass independent detection efficiency.* Proteomics Vol. 1 **1** (2001) 66.

[53] G. Westmacott et al., Proceedings ASMS Conference June 1999, Dallas USA 2000.

[54] Th. Nussbaumer, Ph. Lerch, E. Kirk, A. Zehnder, R. Fuchslin, P.F. Meier and H.R. Ott, *Quasiparticle diffusion in tantalum using superconducting tunnel junctions* Phys. Rev. B **61** (2000) 9719.

[55] A. Zehnder, *Response of superconductive films to localized energy deposition.* Phys. Rev. B **52** (1995) 12858.

[56] J.J.Chang and D.J. Scalpino, *Kinetic-equation approach to nonequilibrium superconductivity.* Phys. Rev. B **15** (1977) 2651.

[57] H. Kraus, F. von Feilitzsch, J. Jochum, R.L Mossbauer, Th. Peterreins and F. Probst, *Quasiparticle trapping in a superconductive detector system exhibiting high energy and position resolution.* Phys. Lett. B **231** (1989) 195.

[58] C.D. Mowry and M.V. Johnston, *Simultaneous Detection of Ions and Neutrals Produced by Matrix-assisted Laser Desorption.* Rapid. Commun. in Mass Spectrom. **7** (1993) 569.

[59] P. Verhoeve, S. Kraft, N. Rando, A. Peacock, A. van Dordrecht, R. den Hartog, D.J Goldie, R. Hart and D. Glowacka, *Soft X-ray response of a 36 pixel superconducting tunnel junction array for high resolution X-ray astronomy.* SPIE **3445** (1998).

[60] P. Verhoeve, S. Kraft, N. Rando, A. Peacock, A. van Dordrecht, R. den Hartog, D.J Goldie, R. Hart and D. Glowacka, *Single optical photon detection with a superconducting tunnel junction* Nature **381** (1996) 135.

[61] D. Twerenbold, *Cryogenic Particle Detectors* Reports in Progress in Physics **59** (1996) 349.

Acknowledgments

I would like to thank Professor Jean-Luc Vuilleumier for giving me the first opportunity to work in experimental physics with his particle group. Later on, I appreciated his support throughout this work.

I thank particulary Dr. Damian Twerenbold for providing me the chance to work on his project as well as for his enthusiasm and competence.

A warmly thank to the mass spectrometry group: Dr. Daniel Gerber, Yvan Gonin, Alexandre Netuschill, Frederic Rossel and Dominique Schenker for their scientific and technical competence as well as their good mood.

I wish also to thank all members of technical staff for innumerable works achieved during this thesis.

Thanks also to my family for their support all along my studies.

Finally, I would like to thank my wife Helena for her love, her patience and her support during this work.